[redacted]

Copy 300
RM L57E31

NACA RM L57E31

NACA

UNCLASSIFIED
NASA T.D. 71,359 5/20/71

RESEARCH MEMORANDUM

FREE-FLIGHT INVESTIGATION AT TRANSONIC SPEEDS OF THE POWER-ON CHARACTERISTICS INCLUDING SOME EFFECTS OF SONIC PROPULSIVE JETS OF A FOUR-ENGINE DELTA-WING CONFIGURATION

By Joseph H. Judd and Ralph A. Falanga

Langley Aeronautical Laboratory
Langley Field, Va.

N71-73439
(ACCESSION NUMBER) 47 (PAGES) (NASA CR OR TMX OR AD NUMBER)
(THRU) None (CODE) (CATEGORY)
FACILITY FORM 602

NATIONAL ADVISORY COMMITTEE
FOR AERONAUTICS
WASHINGTON
August 16, 1957

[redacted]

[redacted]

NATIONAL ADVISORY COMMITTEE FOR AERONAUTICS

RESEARCH MEMORANDUM

FREE-FLIGHT INVESTIGATION AT TRANSONIC SPEEDS OF THE POWER-ON CHARACTERISTICS INCLUDING SOME EFFECTS OF SONIC PROPULSIVE JETS OF A FOUR-ENGINE DELTA-WING CONFIGURATION

By Joseph H. Judd and Ralph A. Falanga

SUMMARY

A free-flight model of a delta-wing configuration with four engines mounted two to a nacelle below the wing was flight tested with rocket turbojet simulators operating from Mach numbers 0.58 to 1.36 and from Reynolds numbers 39×10^6 to 97×10^6; with jets off the Mach numbers ranged from 1.20 to 1.36. Jet-exit static-pressure ratios were about 2.7 for jet-on flight. At Mach number 0.58 the wing static-pressure coefficients were small and appeared to change little between jet-on and jet-off flight. At supersonic speeds, jet-on wing pressure coefficients alternated between positive and negative values. Jet-on flight at Mach number 1.3 was at a nose-down trim angle of attack caused by the pressure field of the jet. A positive increment in lift coefficient was produced by the jet pressure field between jet-on and jet-off flight at Mach number 1.3.

INTRODUCTION

The study of the effect of the flow field about a propulsive jet on flat-plate pressure distribution (refs. 1, 2, 3, and 4) and on tail surfaces (refs. 5 and 6) has shown that appreciable forces and moments may result from jet interference. Since the airplane flow field is warped by curvature of wing and component interferences, appreciable difference in jet effect may result between simple flat plates and an airplane configuration. For this reason, flight tests of a complete four-jet bomber model were made to measure the wing static-pressure distribution behind the jet exits and to compare the changes in measured trim of the configuration with the loads induced by the jet exhaust. This investigation was performed by the Langley Pilotless Aircraft Research Division as part of a program to study various aspects of the effect of a sonic propulsive jet on lift, drag, and stability of airplane configurations.

[redacted]

The airplane configuration selected for this test was a tailless bomber configuration which had a plane 60° delta wing mounted in a shoulder position on a body of revolution. Four rocket motors, modified to simulate the exhaust of turbojet engines and mounted in pairs, were suspended below the wing on pylons.

The flight test was made at the Langley Pilotless Aircraft Research Station at Wallops Island, Va. The Mach number range of these tests was from 0.56 to 1.36 and the Reynolds number range was from 39×10^6 to 97×10^6.

SYMBOLS

A	cross-sectional area, sq ft
$\bar{c}$	wing mean aerodynamic chord, ft
$C_{p,f}$	fuselage pressure coefficient, $\frac{p_f - p_\infty}{q}$
$C_{p,w}$	wing pressure coefficient, $\frac{p_w - p_\infty}{q}$
$C_{p,w,i}$	wing pressure coefficient, where i refers to orifice number, $\frac{p_{w,i} - p_\infty}{q}$
C_L	lift coefficient, Lift/qS
C_{L_α}	lift-curve slope, dC_L/d_α, per deg
$C_{L,T}$	trim lift coefficient
C_m	pitching-moment coefficient, measured about model center of gravity
C_Y	lateral-force coefficient, Lateral force/qS
$C_{Y,T}$	trim lateral-force coefficient
C_{Y_β}	lateral-force slope, $dC_Y/d\beta$, per deg

[redacted]

C_{m_α} static-stability derivative, $dC_m/d\alpha$, per deg

C_n yawing-moment coefficient about center of gravity

$C_{m_q} = \frac{dC_m}{d\left(\frac{\dot{\theta}\bar{c}}{2V}\right)}$, per radian

$C_{m_{\dot{\alpha}}} = \frac{dC_m}{d\left(\frac{\dot{\alpha}\bar{c}}{2V}\right)}$, per radian

$C_{m_q} + C_{m_{\dot{\alpha}}}$ longitudinal damping derivatives, per radian

C_{n_β} directional stability derivative, $dC_n/d\beta$, per deg

d_j diameter of jet at nozzle exit

I_y moment of inertia in pitch about model center of gravity, slugs-ft^2

I_z moment of inertia in yaw about model center of gravity, slugs-ft^2

l fuselage length, ft

M free-stream Mach number

N_{Re} Reynolds number based on wing mean aerodynamic chord

$P_{e,n}$ jet-exit static pressure, where n refers to motor number, lb/sq ft

p_f fuselage static pressure, lb/sq ft

p_w wing static pressure, lb/sq ft

$p_{w,i}$ wing static pressure, where i refers to orifice number, lb/sq ft

p_∞ free-stream static pressure, lb/sq ft

P_α period of short-period longitudinal oscillation, sec

[redacted]

P_β	period of lateral oscillation, sec
q	free-stream dynamic pressure, $\frac{1}{2}\rho V^2$, lb/sq ft
r	radius of equivalent body of revolution, ft
S	total plan-form area, sq ft
t	time from launch, sec
$t_{1/2,\alpha}$	time required for short-period longitudinal oscillation to damp to one-half amplitude, sec
$t_{1/2,\beta}$	time required for lateral oscillation to damp to one-half amplitude, sec
V	velocity, ft/sec
W	weight of model, lb
x	longitudinal station measured parallel to fuselage center line, ft
x_{ac}	distance from leading edge of mean aerodynamic chord to aerodynamic center, percent mean aerodynamic chord, positive rearward
x/d_j	longitudinal distance from nozzle exit
$x/\bar{c}$	longitudinal distance from leading edge of $\bar{c}$ to center of gravity
$z/\bar{c}$	vertical distance from fuselage center line to center of gravity
z/d_j	vertical distance from exit nozzle to wing surface
α	angle of attack at center of gravity, measured from fuselage center line, deg
α_T	trim angle of attack, deg
β	angle of sideslip at center of gravity, measured from fuselage center line, deg
β_T	trim angle of sideslip, deg

[redacted]

θ angle of pitch at model center of gravity, measured from fuselage center line, radians

$\dot{\theta} = d\theta/dt$ radians/sec

ρ air density, slugs/cu ft

MODEL AND APPARATUS

Model

A three-view drawing and photographs showing different views of the test configuration are shown in figures 1 and 2, respectively. The basic geometric parameters of the test configuration are given in table I. The present test configuration was a modified 60° delta-wing—body combination with four simulated turbojet engines arranged in two twin-engine nacelles and mounted on pylons suspended from the lower surface of each wing panel. The present test configuration thus represented a four-engine delta-wing airplane configuration with no horizontal tail.

The test configuration was designed to have a smooth distribution of projected average cross-sectional area, assuming air flow through the nacelles, at $M = 1.20$ for the conditions of jet off. The basic area distribution used for design of the test configuration was obtained from a parabolic body of revolution with fineness ratio 7.8 and a maximum diameter at the 60-percent body station. The method of "hoops" described in reference 7 was used to obtain the average projected areas of the external components of the configuration at $M = 1.2$, and these component areas were subtracted from the initial parabolic body. Thus, the test configuration had a contoured fuselage as shown in figure 1 and coordinates as shown in table II. The normal cross-sectional-area distribution for the test configuration with nacelle inlets faired to a solid ogival nose and nacelle inlets open are presented in figure 3. For the nacelles open, an area ratio of inlet to nacelle frontal area of 0.33 was used. The basic parabolic body is also presented in this plot and this area distribution is equivalent to the configuration with nacelles open.

The wing of the NACA 65A004 airfoil section had 60° sweepback on the leading edge, 10° sweepforward on the trailing edge with rounded wing tips, and was located at shoulder height on the fuselage at 1° 10' incidence angle to the fuselage center line. The total plan-form area was 24.06 square feet and the aspect ratio was 2.10. Airfoil coordinates are given in table III. The model had two thin vertical fins of hexagonal airfoil section with the leading-edge sweepback 60° and the trailing-edge 49°.

The nacelles and pylon are shown in figure 4 and nacelle ordinates are presented in table IV. Basically the nacelle consisted of two contiguous boattail bodies of revolution with fairing between. The nacelle jet exits were located below the wing surface, $z/d_j = 1.68$ and at a longitudinal station of 0.68 of the mean aerodynamic chord. The nacelle pylon of NACA 65A006 airfoil section had a sweepback angle of 67° and the leading edge of the pylon intersects the leading edge of the wing. The ordinates of the airfoil and the mounting ordinates (measured from the center line of the wing) are given in table V.

Turbojet Simulator

A drawing of a typical turbojet simulator, designed according to reference 8, is shown in figure 5. The engines consisted essentially of a dual headcap, a combustion chamber which housed the solid propellant and igniter, a flow-control nozzle, and a convergent sonic exit section. A Cordite SU/K propellant grain generated the exhaust gases to simulate a current full-scale turbojet with afterburner operating at Mach number of 1.20 and an altitude of 35,000 feet. The jet exit diameter was 3.375 inches with a jet area of 0.0621 square foot and the jet base diameter was 3.438 inches with a jet base area of 0.0645 square foot. The engines had a 5° 5' conical boattail angle and one nozzle static-pressure tube per nacelle.

Propulsion and Equipment

In addition to the four turbojet simulator rockets suspended below the wing, a HPAG rocket was installed at the fuselage center line to provide additional thrust. It was necessary to incorporate this rocket (HPAG) in order that the test Mach number range could be achieved. A single 6.25-inch Deacon rocket motor was used to boost the model to high subsonic speed. Figure 6 is a photograph of model and booster on a zero-length launcher.

Instrumentation

Sixteen instruments were carried within the model. The angle of attack and angle of sideslip were measured by an air-flow direction indicator located on a sting ahead of the nose of the model. (See fig. 1.) The longitudinal accelerometer was located at station 33.0 on the center line of the fuselage; whereas, the normal and transverse accelerometers were located at station 69.0, approximately at the center of gravity, and about 3.0 inches from the fuselage center line. Eight static-pressure orifices were installed in the lower surface of the right wing panel as shown in table VI. These orifices were in line with the center line of the inboard turbojet simulator (39.7 percent of the wing semispan) and

[redacted]

were located downstream of the nozzle exit. The fuselage pressure orifice was at station 115 and in the same horizontal plane as the center line of the fuselage. This location is shown on table VI. One motor-nozzle static-pressure orifice was used for each pair of engines. The location of these motor-nozzle static-pressure orifices is shown in figure 5.

An NACA 10-channel telemeter, located in the nose section of the fuselage, continuously transmitted measurements of angle of attack, angle of sideslip, normal accelerations, longitudinal accelerations, transverse accelerations, fuselage static pressure, and one motor-nozzle static pressure, and the telemeter intermittently transmitted measurements of one motor-nozzle static pressure and eight wing static pressures. Each switched channel had a frequency of data transmissions of two cycles per second.

Ground instrumentation consisted of a CW Doppler velocimeter, an NACA modified SCR-584 tracking radar, and a rawinsonde.

TESTS

Preflight Tests

Before the model was free-flight tested, weight, center-of-gravity, and inertia characteristics were measured. The model was also suspended by shock chords and shaken by means of an electromagnetic shaker to determine the structural natural frequencies of the model. The results from these preflight tests are listed in table I.

One of the turbojet simulators used on the flight model was statically tested in the Langley rocket test cell. During this preflight test the motor-nozzle static pressure and thrust were measured. These test results agreed with the motor design calculations. By using these data and the existing sea-level conditions, a calibration curve of the jet-exit static pressure as a function of the motor-nozzle static pressure was obtained for the purpose of evaluating the performance of the turbojet simulators in flight.

Flight Tests

The model was launched from a zero-length launcher (fig. 6). A single ABL Deacon rocket motor boosted the model to a subsonic Mach number of 0.645. The booster and the model decelerated for about 1/2 second before the HPAG rocket and four turbojet simulators started thrusting simultaneously. The model was accelerated to a peak Mach number of 1.36

at which time the HPAG rocket stopped thrusting and the turbojet simulators continued thrusting for approximately 1/2 second longer. The magnitude of the thrust from the simulators was not large enough during the remaining jet-on phase to overcome the drag. After the simulators stopped thrusting the model decelerated and was tracked until splash. Jet-off pressure-distribution data were obtained during the decelerating flight before separation of model from booster and after turbojet simulators stopped thrusting. Jet-on data were obtained during the firing of the HPAG rocket and turbojet simulators. The model was disturbed in pitch when: (1) the HPAG rocket and simulators started thrusting, (2) the model passed through a Mach number of 1.0, (3) the HPAG rocket stopped thrusting, and (4) the simulators stopped thrusting. The model was disturbed in yaw when: (1) the HPAG rocket and simulators started thrusting and (2) the simulators stopped thrusting. The time histories of model velocity, Mach number, dynamic pressure, and air density are shown in figure 7. The variation of the Reynolds number (based on wing mean aerodynamic chord) with Mach number for jet-on and jet-off flight is presented in figure 8. During jet-on flight the model weight, moment of inertia in pitch and yaw, and the longitudinal and vertical locations of the center of gravity changed as the rocket fuel burned. The variations of these quantities with time are given in figure 9. The variation of the ratio of jet-exit static pressure to free-stream static pressure with Mach number for the turbojet simulators is shown in figure 10.

Analysis

Model velocity, obtained with the velocimeter, was corrected for flight-path direction and wind velocity obtained from rawinsonde measurements. Measurements of the air-flow direction indicator were corrected according to the method of reference 9 for model pitching velocity. Accelerometer corrections due to pitching rate were negligibly small.

The method of obtaining lift and longitudinal stability coefficients and derivatives from transient longitudinal disturbances is given in reference 10. Reference 10 utilizes two degrees of freedom - pitch and vertical displacement. An examination of the flight records indicated that over most of the test range there appeared to be no interaction between the lateral and longitudinal oscillations of model; thus the separation of the two modes of oscillation was justified.

RESULTS AND DISCUSSION

Wing Pressure Coefficients

The variations of wing pressure coefficients with Mach number for jet-on and jet-off flight are presented in figure 11. Since the model

[redacted]

had negative lift and nose-down pitching moment, the model dived into the ocean sooner than expected; thus, the jet-off lower Mach number was limited to 1.20. Jet-off data from $M = 0.56$ to 0.58 were obtained during coasting flight before the model separated from the booster. Before separation the trim angle of attack of the model-booster combination was -4.0°; whereas immediately after separation when the rocket motors of the model fired, the trim angle of attack was -1.2°. Orifice number 1 which was located approximately at the exit nozzle was the only wing pressure orifice that indicated an appreciable difference in wing pressure coefficient (from jet-off $C_{p,w} = -0.03$ to jet-on $C_{p,w} = 0.13$). The changes in wing pressure coefficient indicated by wing orifices 2 to 8 were small and masked by the difference in wing angle of attack which should increase the pressure coefficients by 0.03 (ref. 11 at $M = 0.40$). The difference between jet-on and jet-off wing pressure coefficients is more pronounced at supersonic speeds.

Appreciable changes in wing pressure coefficients with Mach number during jet-on flight were noted at transonic speeds. These changes are caused by the increased efficiency of transmission of pressure disturbances from the jet through sonic and supersonic streams. The abrupt changes in wing pressure coefficients noted at orifices 3, 4, 7, and 8 were caused by the passage of shock waves over the orifices. In general it can be stated that chordwise wing pressure coefficients above the jet are approximately the same magnitude at subsonic speeds as jet-off values since disturbances from shock waves within the jet are not propagated to the wing. At supersonic speeds the wing pressures appear to vary proportionately as the pressure along the jet boundary. This corresponds to the jet interference on a flat plate (ref. 3).

The exhausting of a gas jet out of a sonic nozzle at a jet static pressure somewhat greater than free-stream static pressure is characterized by the expansions and recompressions of the jet as described in reference 12. These jet expansions and recompressions cease for a sonic jet exhausting into a static or subsonic stream as the ratio of jet total to static pressure approaches that for sonic flow and cease for a sonic jet exhausting into a supersonic stream when the jet total to static pressure ratio approaches that of the supersonic stream. The formation of the shock wave when the initial expansion of the jet from the nozzle comes in contact with the supersonic stream will be called the exit shock, whereas any shock waves originating in the jet and penetrating the jet boundary will be called jet shocks.

The variations of jet-on wing pressure coefficients along the wing chord above the inboard jet engine are presented in figure 12 for several Mach numbers. At subsonic speeds (fig. 12(a)) pressure coefficients vary along the wing chord as in a standing wave and are similar to the pressure distribution along the jet but are of much smaller amplitude. At

[redacted]

Mach number 0.9 (fig. 12(a)) compressibility effects become apparent and a strong disturbance occurred at x/d_j near 4. This disturbance is due to the second jet shock and tends to decrease in magnitude as the Mach number increases. (See figs. 12(b) and (c).) At Mach number 0.95 (fig. 12(b)) the first jet shock wave at x/d_j near 1.7 starts to produce a strong effect on the wing pressure distribution. This first jet shock continues to produce a strong disturbance to Mach number 1.30. The expansion of the jet at the exit causes a compression in the surrounding stream and a large increase in pressure coefficient over the test Mach number range. However, the forward location of the exit shock cannot be determined until at the higher Mach numbers (fig. 12(c)) because of wing orifice location. At Mach number 1.30 the profile of wing pressure coefficient resembles that on the flat plate (ref. 3).

The jet-off variations of pressure coefficients are also shown at Mach number 0.58 (fig. 12(a)) and at Mach number 1.30 (fig. 12(c)). At $M = 0.58$ the jet-off pressure coefficients (fig. 12(a)) are lower than the jet-on values. However, the difference in trim angle of attack between jet-on and jet-off flight at $M = 0.58$ was -2.8°, and reference 11 indicates that the difference in trim angle of attack would account for the difference in wing pressure coefficients. At $M = 1.30$, the difference between jet-off and jet-on pressure coefficients (fig. 12(c)) alternates between positive and negative values along the wing chord. However, the difference in angle of attack between jet-on and jet-off flight was 1.6°. This difference in angle of attack produces an increment of approximately 0.068 in pressure coefficient. A comparison of the difference between jet-on and jet-off pressure coefficients at $M = 1.30$ and that of reference 3 at $M = 1.39$ shows that the general shape of the pressure distributions is similar, but the present data have greater positive increments because of the inclination of the jet toward the wing.

Fuselage Pressure Coefficient

The variation of a fuselage pressure coefficient with Mach number is plotted in figure 13. At the maximum Mach number of these tests, there was 1/2 second when the fuselage rocket stopped firing and the wing motors continued. Since both fuselage and wing motors fired to this Mach number, it is only possible to isolate the effects of the fuselage and the wing rockets at $M = 1.35$. However, the positive values of pressure coefficient below $M = 1.0$ were probably due to the pressure field of the fuselage motor. (See ref. 13.) The decrease above $M = 1.0$ with Mach number was probably a result of the base shock wave moving rearward on the fuselage because of the increasing energy of the external flow field. However, at $M = 1.35$ no change in fuselage pressure coefficient was observed when the fuselage motor stopped firing.

[redacted]

Airplane Aerodynamic Characteristics

The longitudinal aerodynamic characteristics obtained from these tests (C_L, C_{L_α}, C_{m_α}, $t_{1/2,\alpha}$, P_α, x_{ac}, and $C_{m_q} + C_{m_{\dot{\alpha}}}$) are plotted in figures 14 to 20. A small amount of lateral data was also obtained (variation of C_Y with β and variations of C_{Y_β}, P_β, C_{n_β}, and $t_{1/2,\beta}$ with M) and plotted in figures 21 to 25. It should be emphasized that the model had a fin below the fuselage which was used to cut down on any Dutch roll tendency of the configuration. Thus the lateral coefficients obtained do not represent those for an airplane configuration.

Airplane Trim

The trim angle of attack and trim angle of sideslip are plotted in figure 26 as a function of Mach number, and the trim lift and lateral-force coefficients are plotted as a function of Mach number in figure 27. The values of β_T and $C_{Y,T}$ were small through the test Mach number range. The differences between jet-on and jet-off flight were small and varied in magnitude about the accuracy of the β indicator. With jet-on, the model trimmed at negative values of α varying from -1.2° to -2.8°. The thrust line of the nacelle motors was located below the center of gravity of the model and, therefore, the thrust gives a nose-up pitching moment. At $M = 1.3$ the nose-up pitching-moment coefficient due to the thrust is 0.0023.

The change in pitching-moment coefficient of the airplane can be obtained by using trim lift coefficients and trim angles of attack together with values of C_{L_α} and C_{m_α}. At $M = 1.3$ the airplane experiences a nose-down pitching moment of -0.016 from jet-off to jet-on condition. Since the nose-up thrust pitching moment is also included, the actual pitching-moment change due to the jet pressure field is -0.018.

Similarly the change in lift of the wing can be obtained by using α_T, $C_{L,T}$, and C_{L_α}. Again at Mach number 1.3 the lift increment due to the jet pressure field is approximately 0.034 at angles of attack close to 0°. By using these values of ΔC_L and ΔC_m, the center of pressure of the jet pressure field was found to be located $0.53\bar{c}$ rearward of the center of gravity and the jet exit is located $0.42\bar{c}$ rearward of the center of gravity. This rearward location of the center of pressure of the jet-induced pressure field is caused by the conical nature of the flow field about the jet exhausts. The intersection of the jet shock with the wing (fig. 12) caused an increase in wing pressure coefficient and contributed the major portion of the lift increment. This increase in pressure coefficient sweeps rearward inboard and outboard of the engine nacelles and moves the center of pressure rearward.

[redacted]

The trim angle of attack decreased at M = 1.0 when the jets were operating. There are at least two causes: one the tendency of unsymmetrical models to change trim angle of attack at transonic speeds and the other the effect of the propulsive jet. Because the jet-off data were incomplete, the magnitude of the contribution of each cannot be determined.

SUMMARY OF RESULTS

A rocket-propelled model of a four-engine delta-wing configuration was flight tested over a Mach number range from 0.58 to 1.36 and Reynolds number range from 39×10^6 to 97×10^6. Four rocket motors, modified to simulate the exhaust of a turbojet, with afterburner were mounted in pairs on pylons hung below the wing. Jet-exit static-pressure ratios over the test range were about 2.7.

Pressure coefficients obtained on the wing downstream of an engine nozzle indicated that wing static-pressure coefficients changed very little between jet-on and jet-off flight at Mach number 0.58. As transonic speed was reached, appreciable changes in jet-on wing pressure coefficients occurred. At supersonic speeds the jet produced jet-on pressure coefficients alternating between positive and negative values along the wing chord as observed in previous tests on a flat plate.

At Mach number 1.30 jet-on flight produced a nose-down trim angle of attack due to pitching moment induced on the wing by the jet pressure field. Operation of the jet at Mach number 1.30 also caused a positive increment in lift coefficient between jet-on and jet-off flight.

Langley Aeronautical Laboratory,
National Advisory Committee for Aeronautics,
Langley Field, Va., May 9, 1957.

[redacted]

REFERENCES

1. Bressette, Walter E.: Investigation of the Jet Effects on a Flat Surface Downstream of the Exit of a Simulated Turbojet Nacelle at a Free-Stream Mach Number of 2.02. NACA RM L54E05a, 1954.

2. Bressette, Walter E., and Faget, Maxime A.: An Investigation of Jet Effects on Adjacent Surfaces. NACA RM L55E06, 1955.

3. Bressette, Walter E., and Leiss, Abraham: Investigation of Jet Effects on a Flat Surface Downstream of the Exit of a Simulated Turbojet Nacelle at a Free-Stream Mach Number of 1.39. NACA RM L55L13, 1956.

4. Englert, Gerald W., Wasserbauer, Joseph F., and Whalen, Paul: Interaction of a Jet and Flat Plate Located in an Airstream. NACA RM E55G19, 1955.

5. Salmi, Reino J., and Klann, John L.: Interference Effects at Mach 1.9 on a Horizontal Tail Due to Trailing Shock Waves From an Axisymmetric Body With an Exiting Jet. NACA RM E55J13a, 1956.

6. Cornette, Eldon S., and Ward, Donald H.: Transonic Wind-Tunnel Investigation of the Effects of a Heated Propulsive Jet on the Pressure Distribution Along a Fuselage Overhang. NACA RM L56A27, 1956.

7. Hoffman, Sherwood, Wolff, Austin L., and Faget, Maxime A.: Flight Investigation of the Supersonic Area Rule for a Straight Wing-Body Configuration at Mach Numbers Between 0.8 and 1.5. NACA RM L55C09, 1955.

8. DeMoraes, Carlos A., Hagginbothom, William K., Jr., and Falanga, Ralph A.: Design and Evaluation of a Turbojet Exhaust Simulator, Utilizing a Solid-Propellant Rocket Motor, for Use in Free-Flight Aerodynamic Research Models. NACA RM L54I15, 1954.

9. Mitchell, Jesse L., and Peck, Robert F.: An NACA Vane-Type Angle-of-Attack Indicator for Use at Subsonic and Supersonic Speeds. NACA TN 3441, 1955. (Supersedes NACA RM L9F28a.)

10. Gillis, Clarence L., Peck, Robert F., and Vitale, A. James: Preliminary Results From a Free-Flight Investigation at Transonic and Supersonic Speeds of the Longitudinal Stability and Control Characteristics of an Airplane Configuration With a Thin Straight Wing of Aspect Ratio 3. NACA RM L9K25a, 1950.

[redacted]

11. Smith, Donald W., and Reed, Verlin D.: A Comparison of the Chordwise Pressure Distribution and Spanwise Distribution of Loading at Subsonic Speeds on Two Triangular Wings of Aspect Ratio 2 Having NACA 0005 and 0008 Sections. NACA RM A51L21, 1952.

12. Prandtl, Ludwig: Essentials of Fluid Dynamics. Hafner Pub. Co., (New York), 1952.

13. Henry, Beverly Z., Jr., and Cahn, Maurice S.: Pressure Distributions Over a Series of Related Afterbody Shapes as Affected by a Propulsive Jet at Transonic Speeds. NACA RM L56K05, 1957.

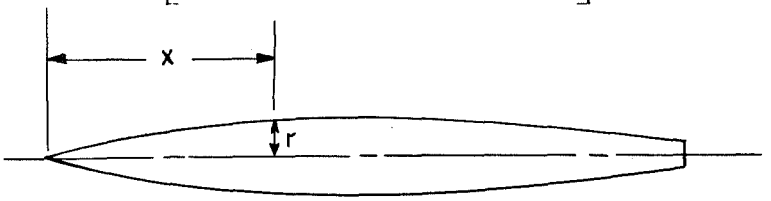
[redacted]

TABLE I.- GEOMETRIC PARAMETERS OF CONFIGURATION

Wing:	
Total plan-form area, sq ft	24.06
Span, ft	7.10
Aspect ratio	2.10
Taper ratio	0
Leading-edge sweepback angle, deg	60
Trailing-edge sweepforward angle, deg	10
Mean aerodynamic chord, ft	4.52
Dihedral, deg	0
Incidence angle (with respect to model center line), deg	1° 10'
NACA airfoil section parallel to free stream	65A004
Fuselage:	
Length, ft	10
Maximum frontal area, sq ft	0.716
Fineness ratio	10.47
Base area, sq ft	0.171
Indentation Mach number	1.2
Nacelles:	
Overall length, ft	4.01
Base area, sq ft	0.065
Jet-exit area per engine, sq ft	0.062
Boattail angle, deg	5° 5'
Maximum frontal area, nacelles, sq ft	0.314
Vertical distance from airplane center line to nacelle center line, ft	0.236
Strut:	
NACA airfoil section parallel to free stream	65A006
Leading-edge and trailing-edge sweepback angle, deg	67
Horizontal distance from airplane center line to strut, percent of semispan	45.8
Vertical fin (both fins):	
Aspect ratio	2.48
Taper ratio, Tip chord/Root chord	0.418
Area, sq ft	3.785
Airfoil section	Trapezoidal
Leading-edge sweep, deg	60
Trailing-edge sweep, deg	49
General:	
Wing-body first bending frequency, cps	79
Wing-body second bending frequency, cps	96
Wing-body third bending frequency, cps	198
Wing bending frequency, cps	244

TABLE II.- FUSELAGE ORDINATES

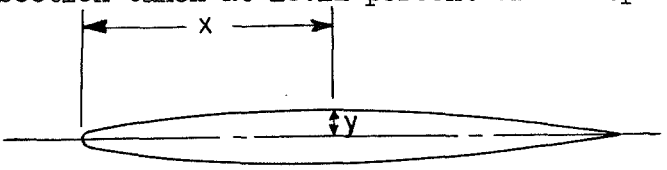
[All dimensions are in inches]



x	r
0	0
.200	.042
.400	.084
1.000	.206
2.000	.410
6.000	1.198
10.000	1.938
14.000	2.634
18.000	3.282
22.000	3.884
26.000	4.438
30.000	4.948
33.687	5.290
34.000	5.400
38.000	5.610
42.000	5.675
46.000	5.745
50.000	5.705
54.000	5.545
58.000	5.115
62.000	4.695
66.000	4.335
70.000	4.100
74.000	3.900
78.000	3.800
82.000	3.780
86.000	3.780
90.000	3.900
94.000	4.080
98.000	4.180
102.000	4.160
106.000	4.010
110.000	3.700
114.000	3.364
115.200	3.270
118.000	3.000
120.000	2.800

TABLE III.- WING ORDINATES

[All dimensions are in inches; coordinates of airfoil section taken at 26.21 percent of semispan]



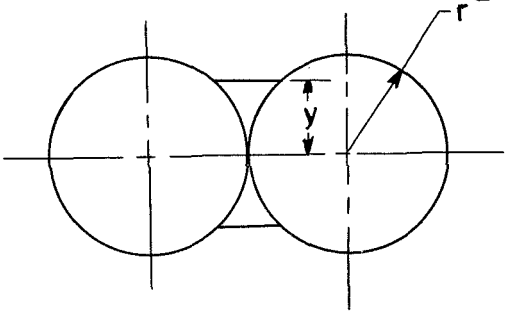
x	y
0	0
.300	.187
.450	.277
.750	.289
1.500	.394
3.000	.526
4.500	.637
6.000	.730
9.000	.878
12.000	.989
15.000	1.074
18.000	1.136
21.000	1.177
24.000	1.198
27.000	1.198
30.000	1.171
33.000	1.120
36.000	1.045
39.000	.950
42.000	.840
45.000	.716
48.000	.580
51.000	.437
54.000	.294
57.000	.149
60.000	.005

Leading-edge radius = 0.061
Trailing-edge radius = 0.006

[redacted]

TABLE IV.- NACELLE ORDINATES

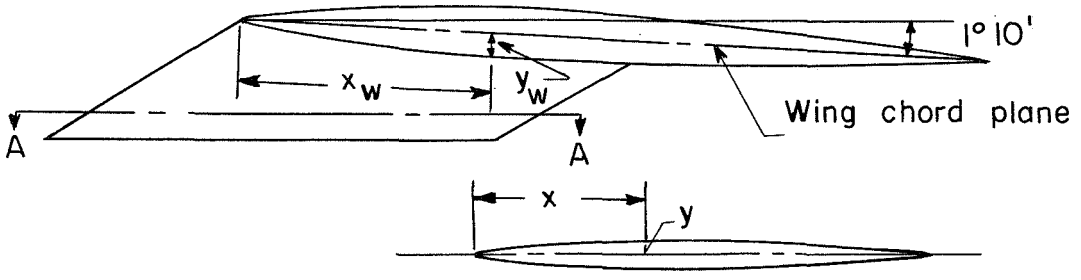
[All dimensions are in inches;
x = 0 at nacelle nose tip]



x	r	y
0	0	0
.250	.175	.200
.625	.440	.360
1.000	.668	.520
2.000	1.170	.876
3.000	1.562	1.180
4.000	1.855	1.410
5.000	2.100	1.590
6.000	2.271	1.730
7.000	2.400	1.830
8.000	2.495	1.880
9.000	2.550	1.915
10.000	2.594	1.938
38.064	2.594	1.938
39.064	2.594	1.885
40.064	2.549	1.836
41.064	2.447	1.795
42.064	2.344	1.543
43.064	2.242	1.383
44.064	2.139	1.212
45.064	2.038	1.016
46.064	1.938	.784
47.064	1.837	.479
47.626	1.760	0
48.064	1.719	-----

TABLE V.- PYLON ORDINATES

[All dimensions are in inches]



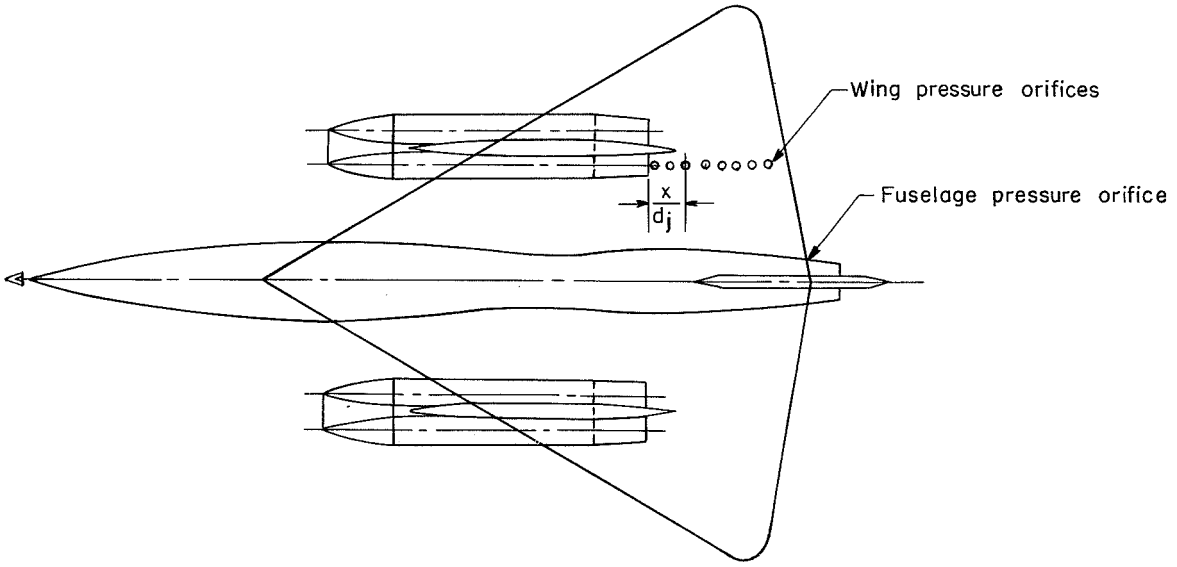
Section A-A

Mounting ordinates taken from wing center line		Airfoil coordinates section A-A	
x_w	y_w	x	y
0	0	0	0
.221	.137	.145	.135
.331	.167	.218	.163
.552	.212	.363	.208
1.104	.290	.725	.284
2.207	.387	1.450	.381
3.311	.469	2.178	.462
4.414	.537	2.900	.529
6.621	.646	4.350	.637
8.828	.728	5.800	.717
11.035	.790	7.250	.779
13.242	.836	8.700	.824
15.449	.866	10.150	.854
17.656	.881	11.600	.869
19.863	.881	13.050	.868
22.070	.862	14.500	.848
24.277	.824	15.950	.810
26.484	.769	17.400	.755
28.691	.699	18.850	.686
30.898	.618	20.300	.605
		21.750	.515
		23.200	.417
		24.650	.314
		26.100	.210
		27.550	.107
		29.000	.038

[redacted]

TABLE VI.- WING ORIFICES

[Located at 39.68 percent of semispan]



Orifice	x/d_j
1	0.0151
2	.964
3	1.643
4	2.304
5	3.072
6	3.720
7	4.490
8	5.150

[redacted]

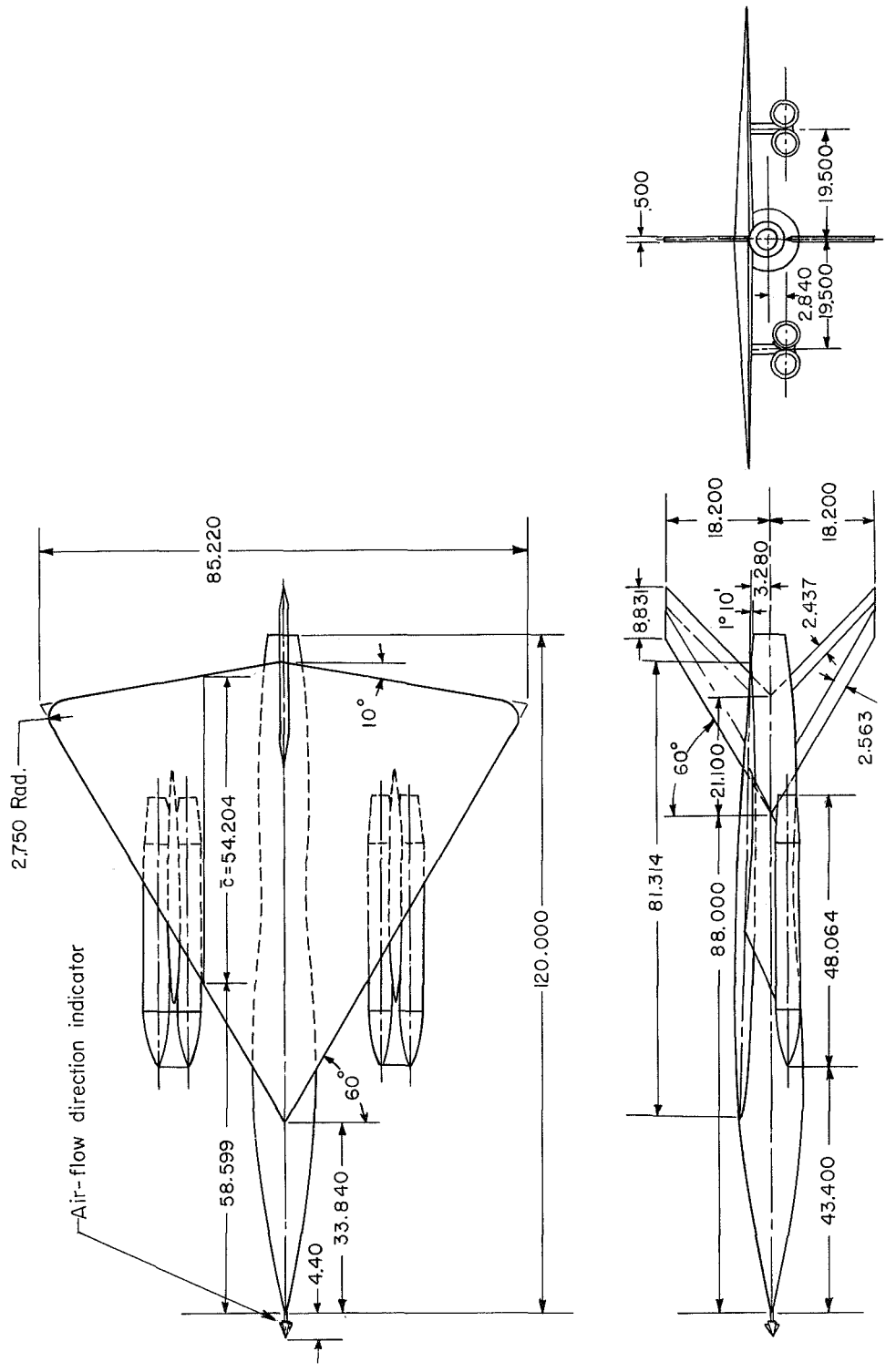
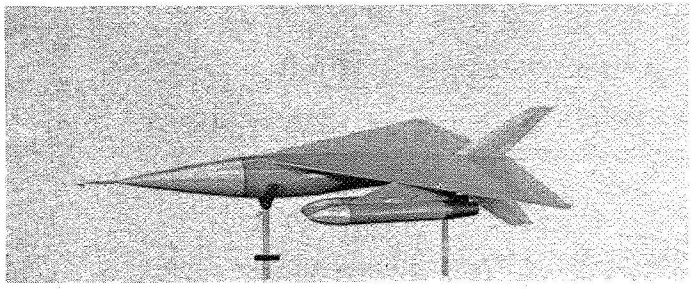
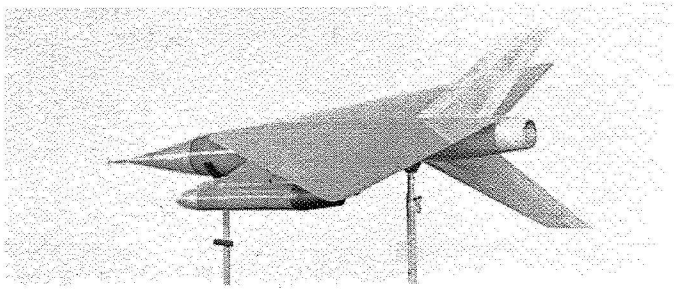


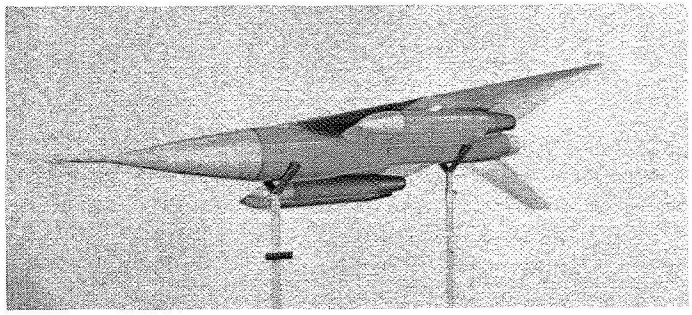
Figure 1.- Three-view drawing of test configuration. All dimensions are in inches.



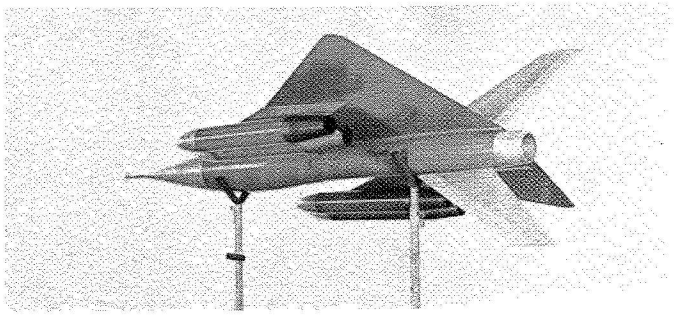
(a) Three-quarter front view of model from top.



(b) Three-quarter rear view of model from top.

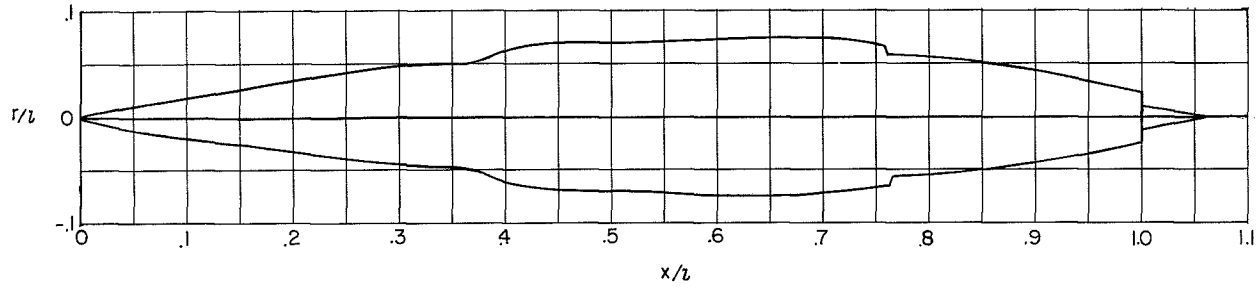


(c) Three-quarter front view of model from below.

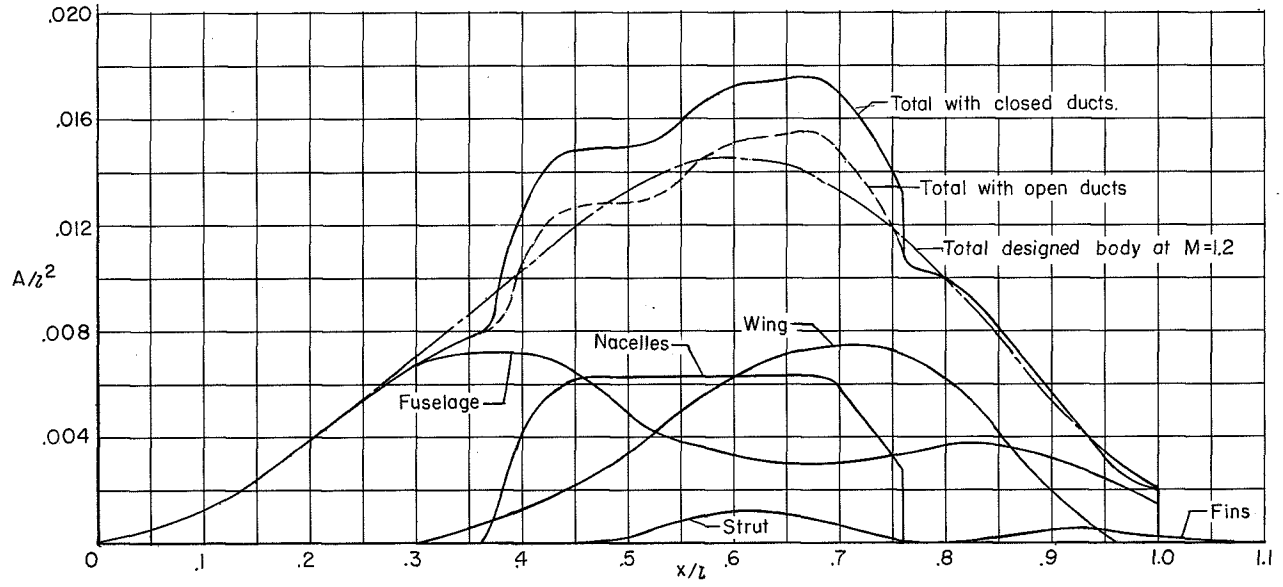


(d) Three-quarter rear view of model from below.

Figure 2.- Photographs of flight model. L-57-1595



(a) Equivalent body of revolution for model.



(b) Cross-sectional area distribution for model.

Figure 3.- Equivalent body of revolution and cross-sectional area distribution for model.

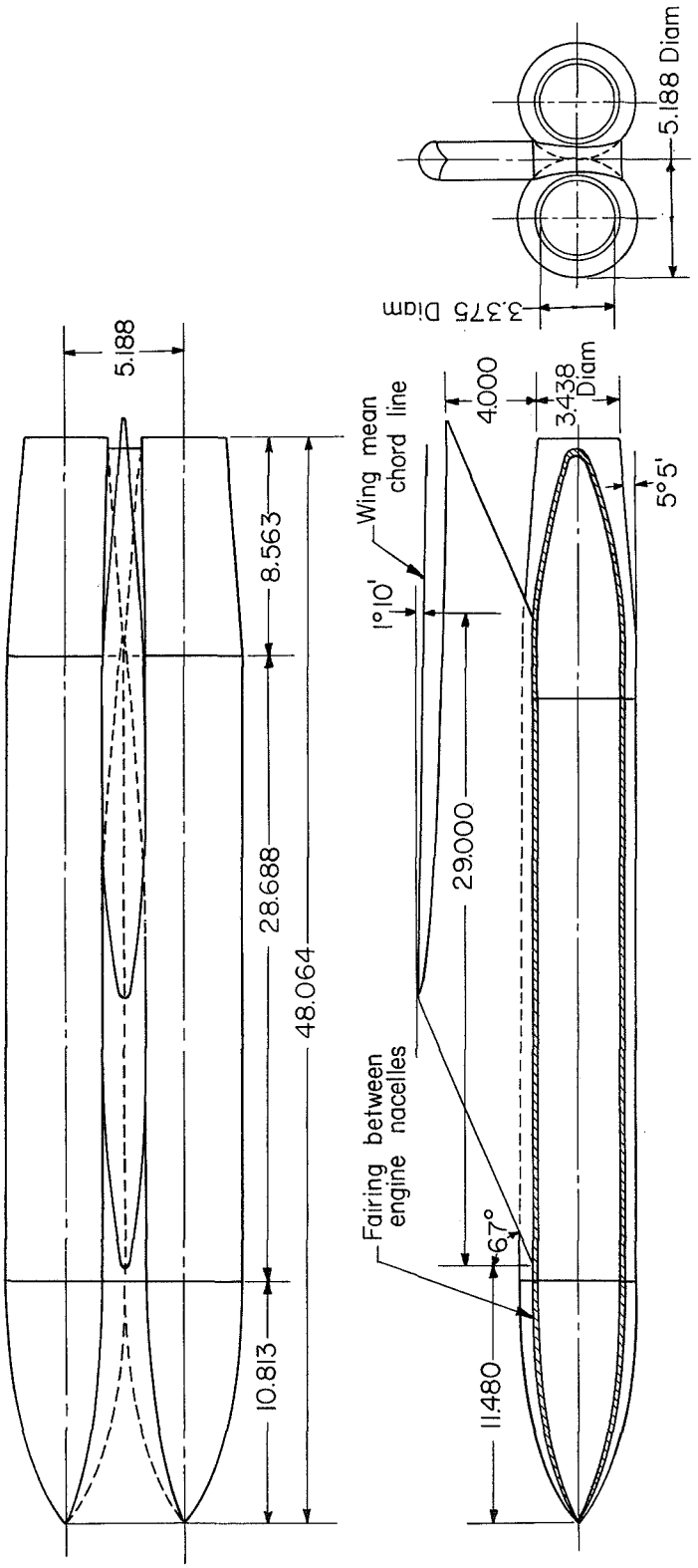


Figure 4.- Drawing of nacelle and pylon. All dimensions are in inches.

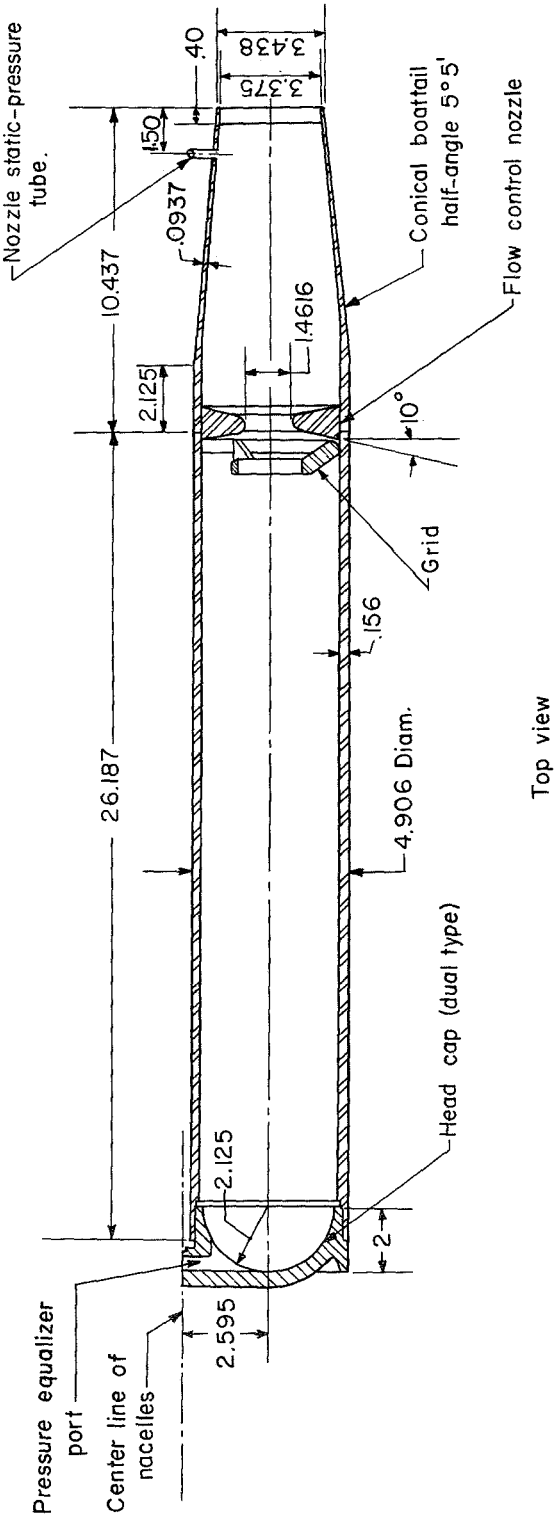


Figure 5.- Drawing of turbojet simulator. All dimensions are in inches.

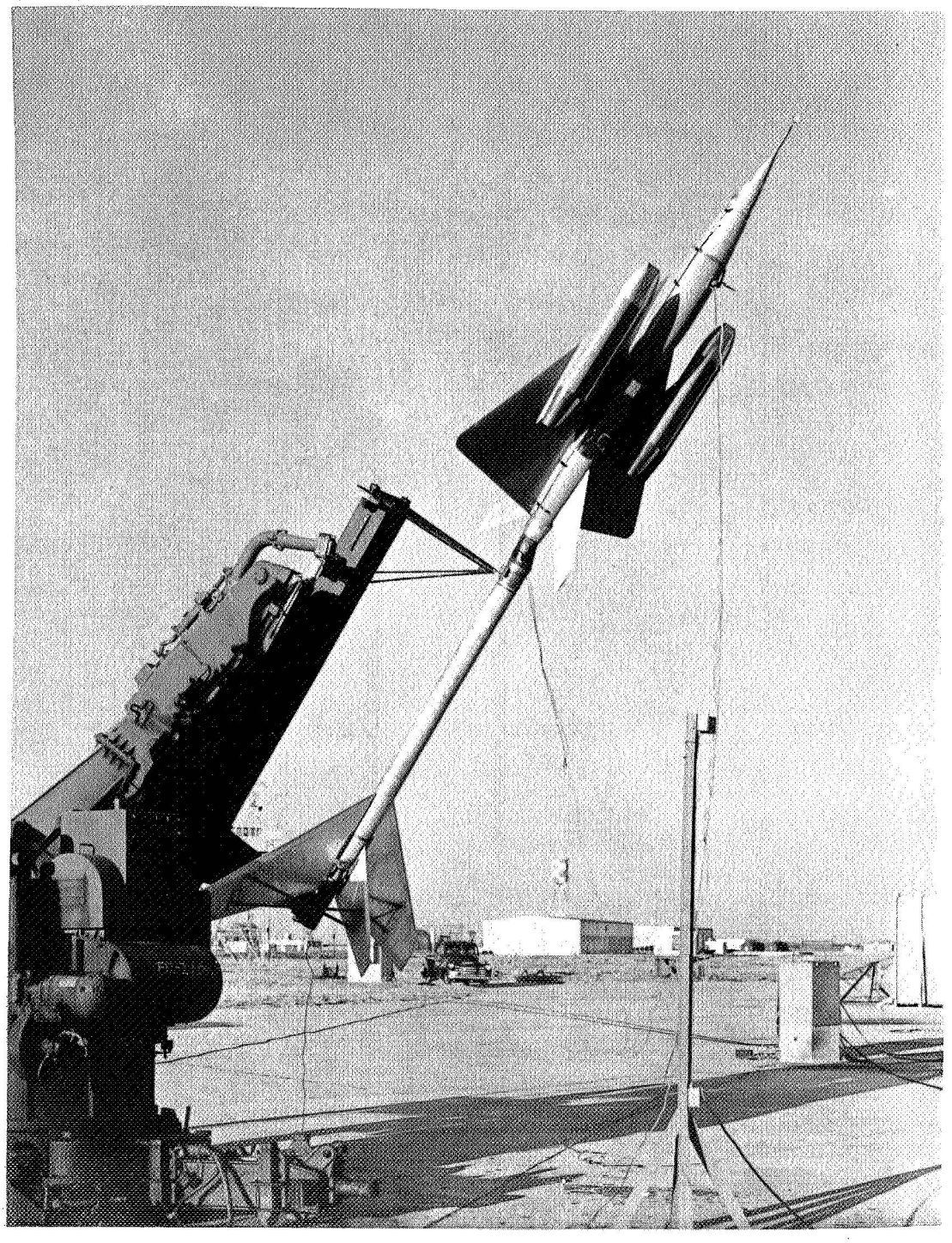
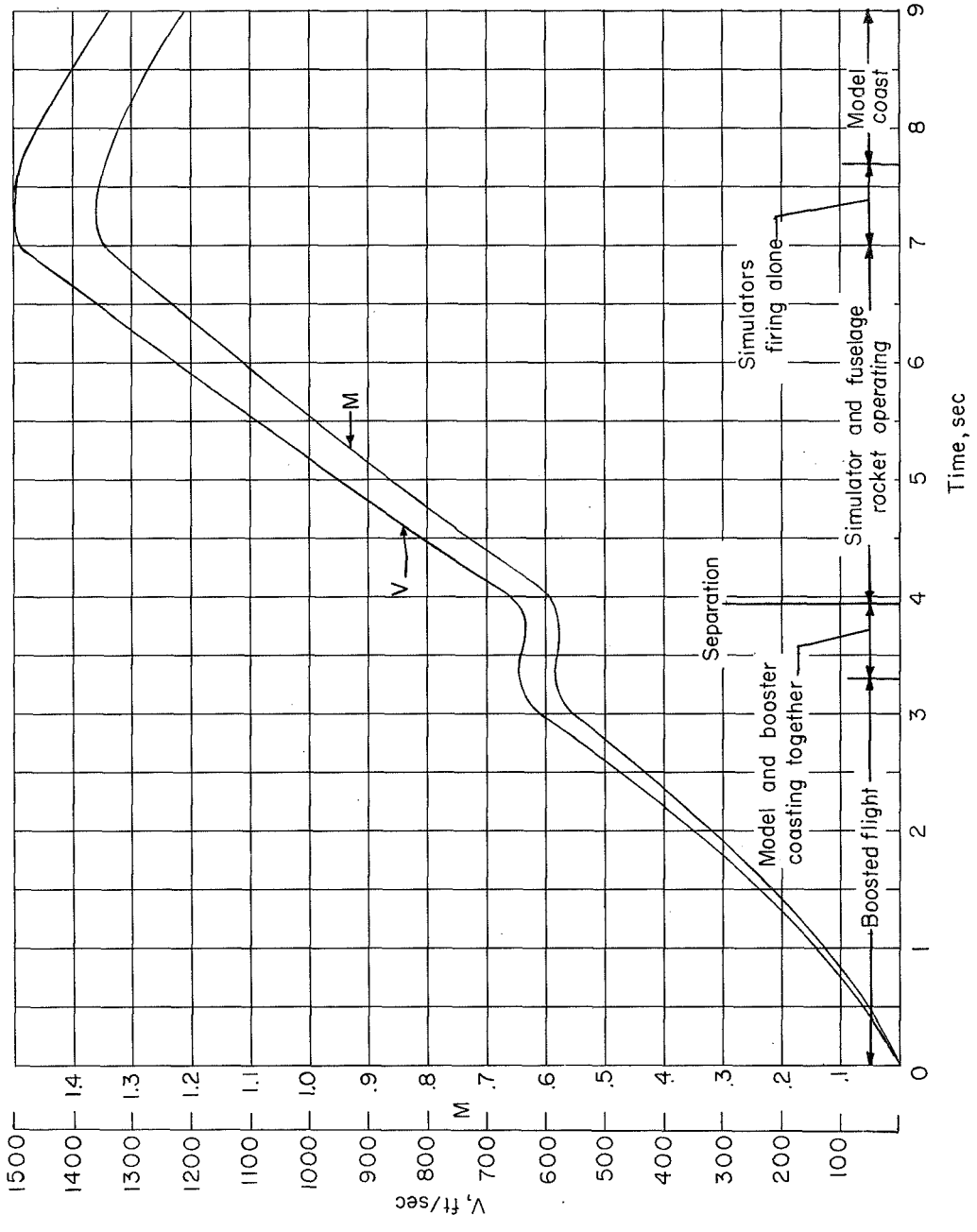


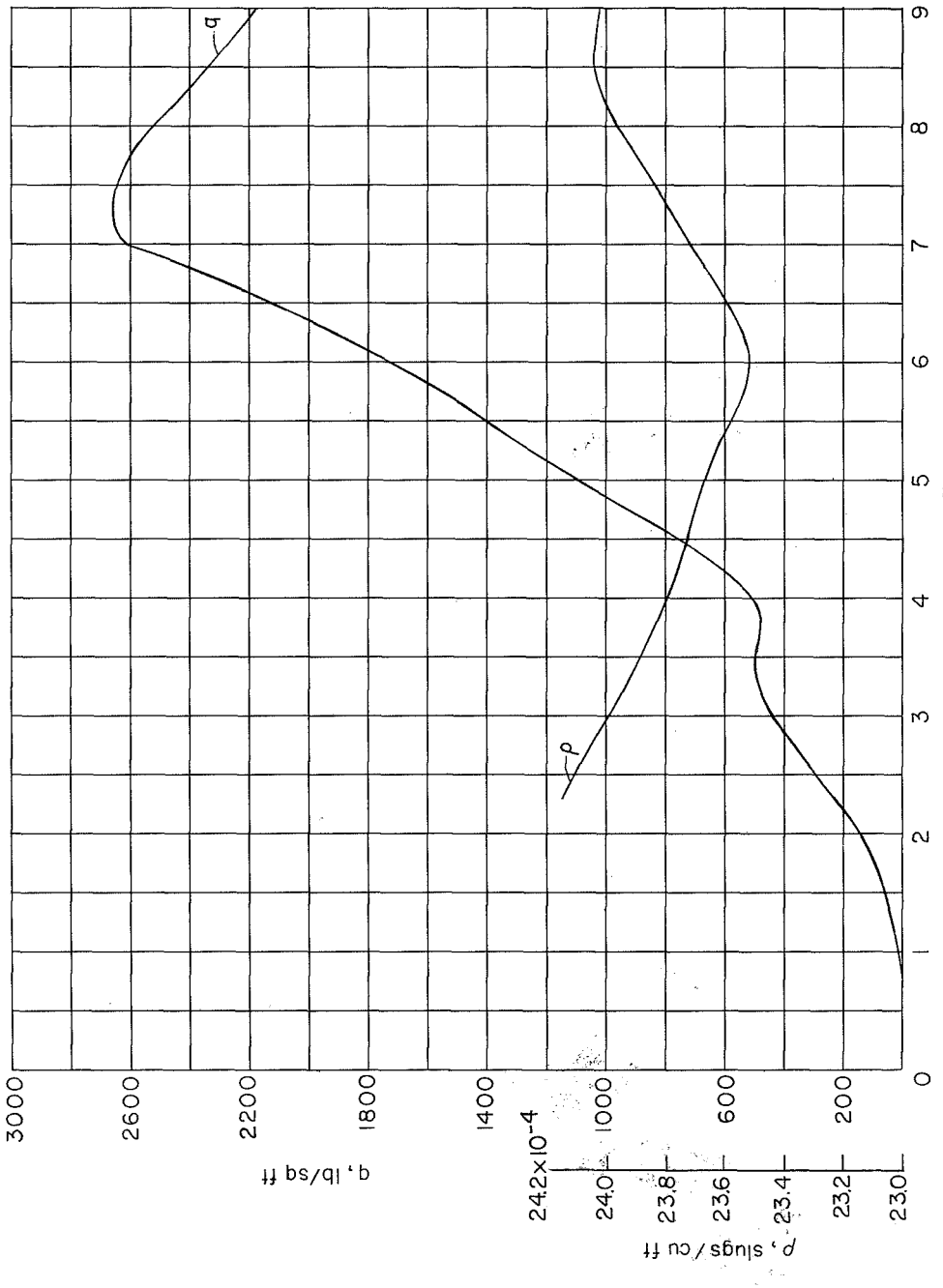
Figure 6.- Model and booster on launcher. L-91901

[redacted]



(a) Variation of velocity and Mach number with time.

Figure 7.- Time history of free-stream test conditions.



(b) Variation of density and dynamic pressure with time.

Figure 7.- Concluded.

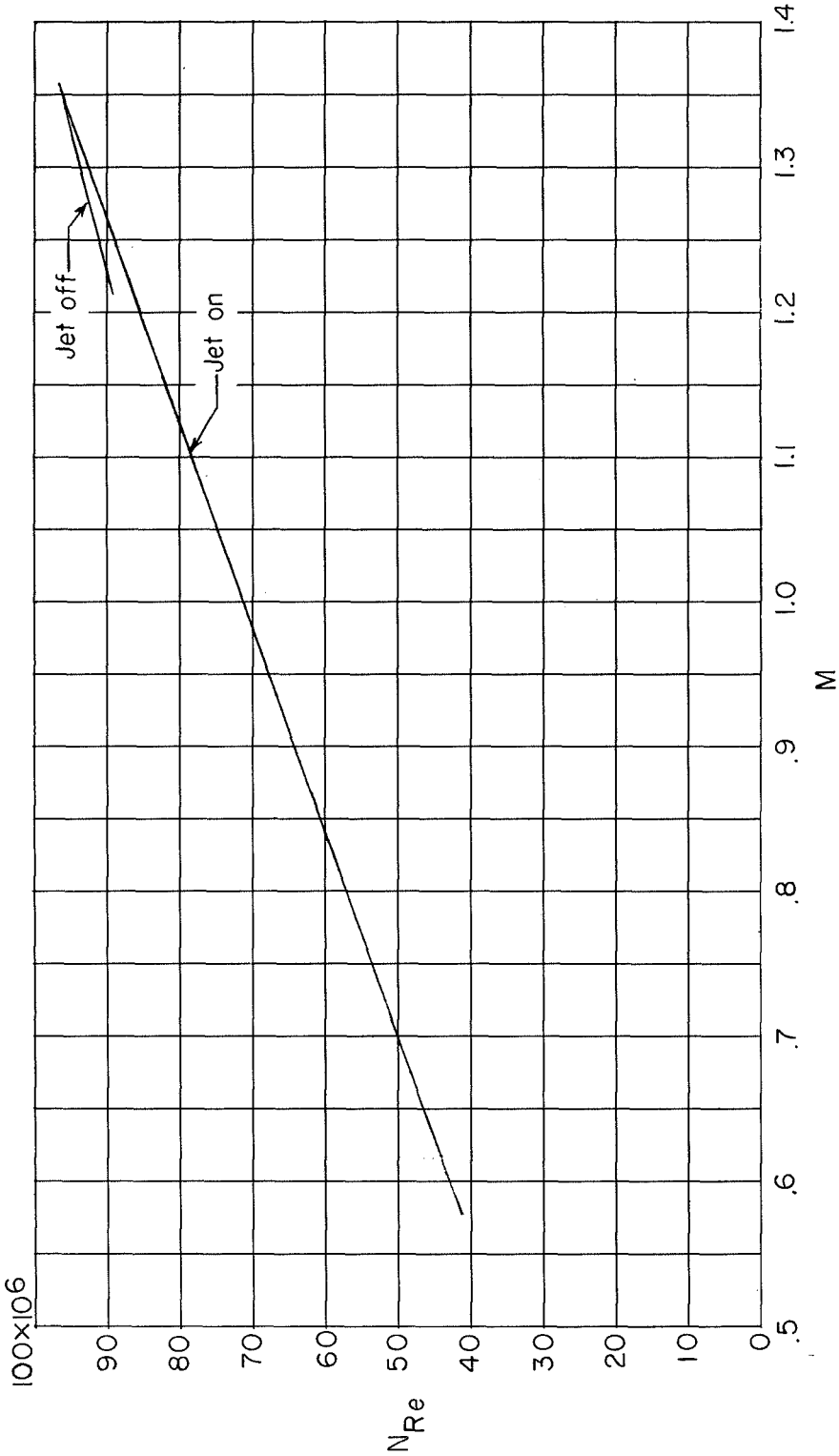
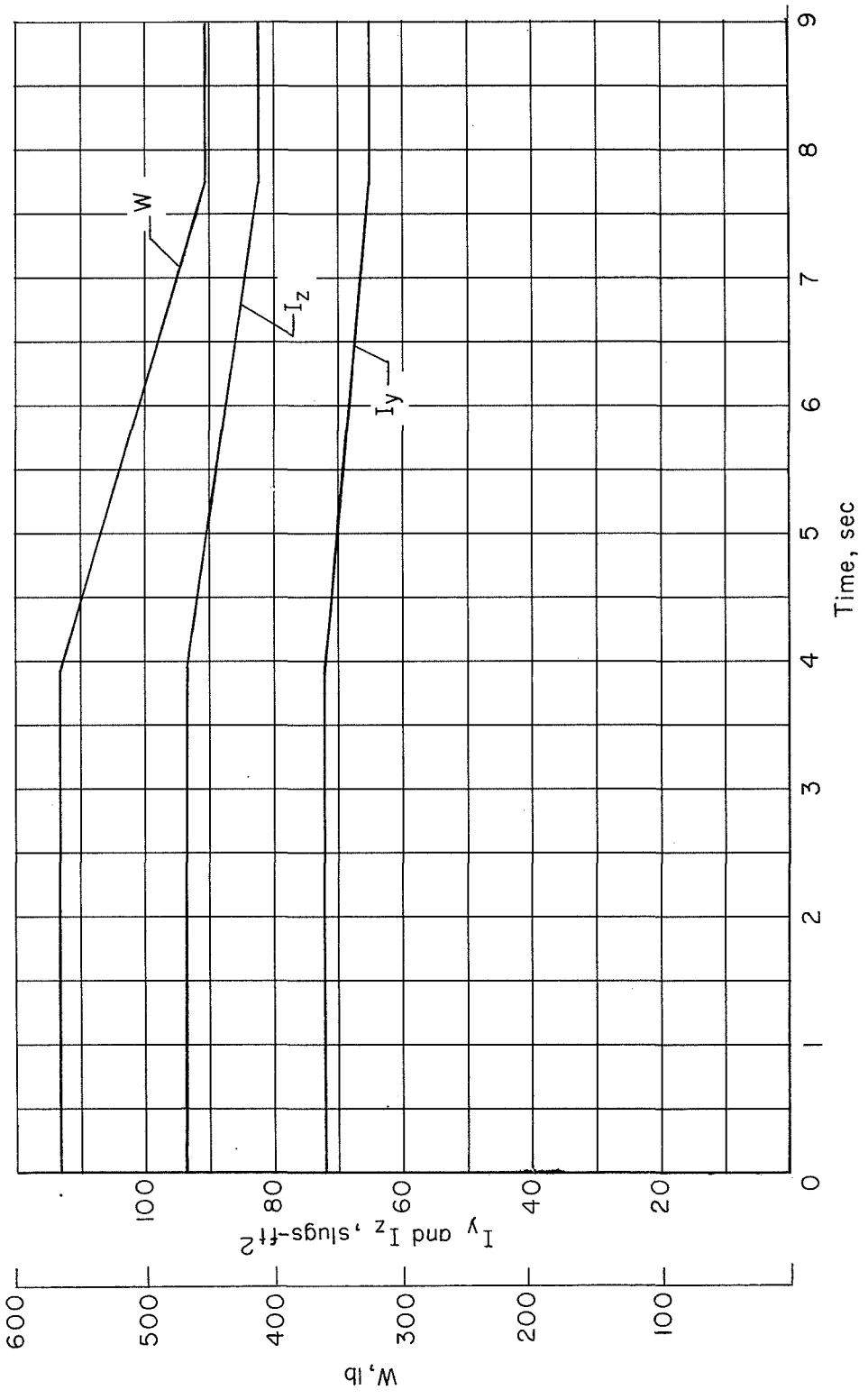


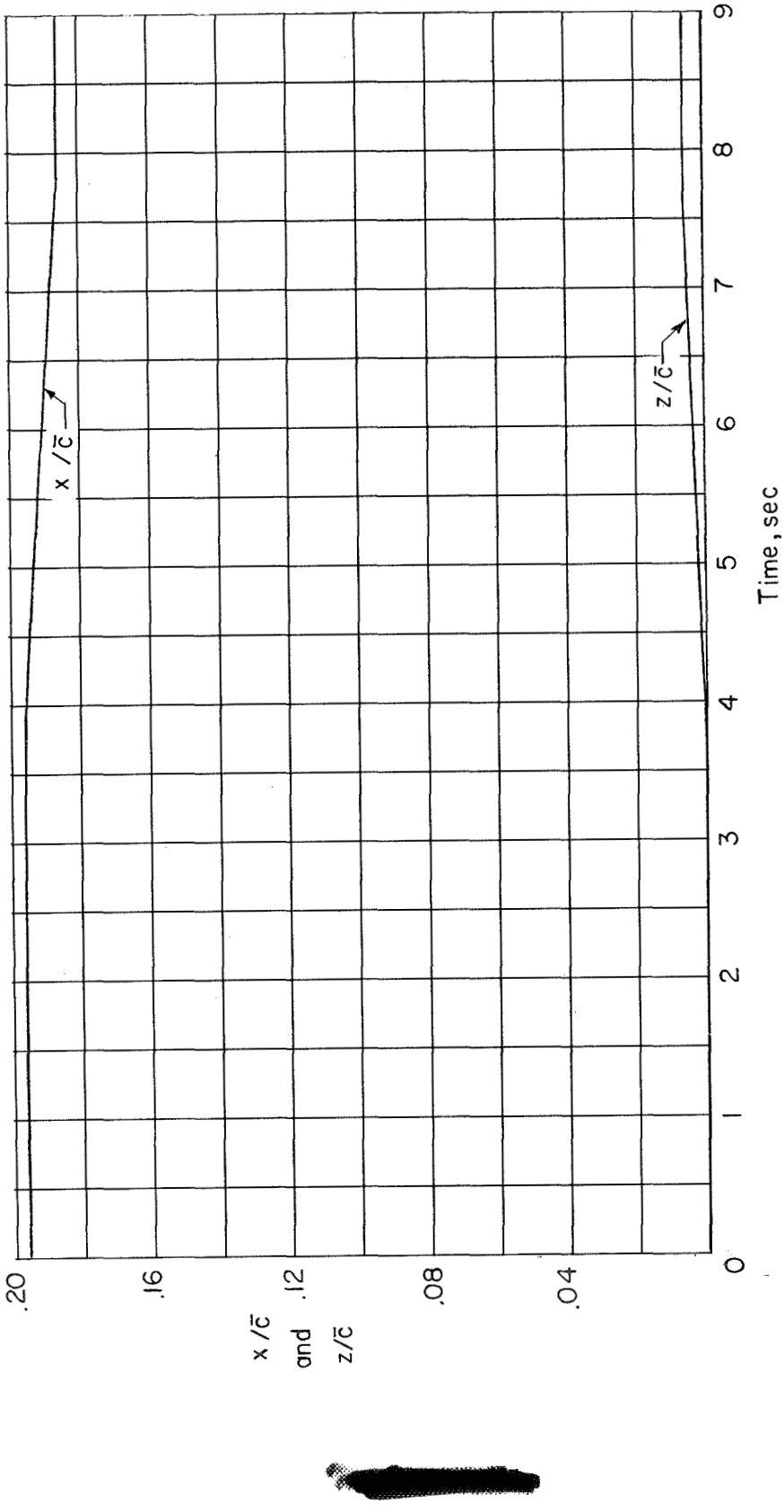
Figure 8.- Variation of Reynolds number, based on wing mean aerodynamic chord, with Mach number.



(a) Variation of model weight and moment of inertia with time.

Figure 9.- Variation of model quantities during flight test.

CLASSIFIED



(b) Variation of model center of gravity with time.

Figure 9.- Concluded.

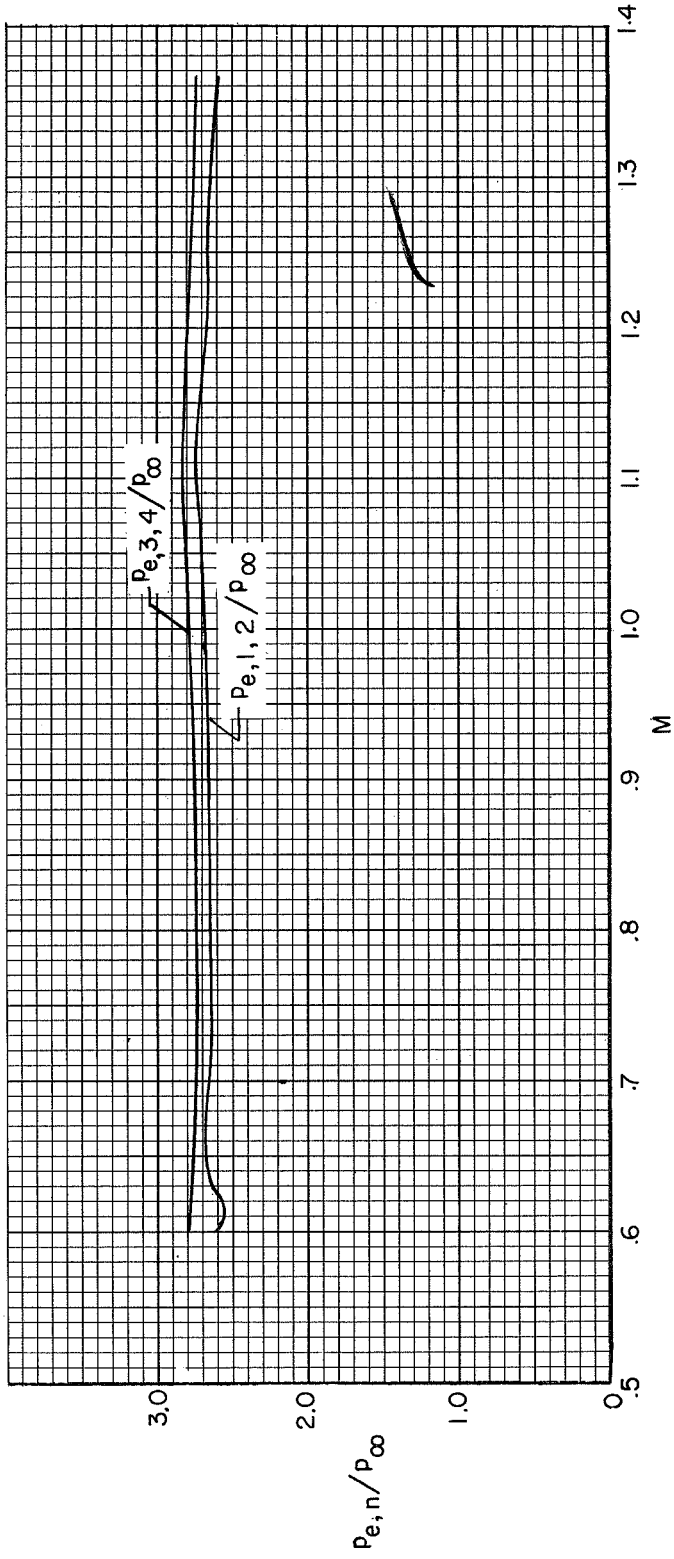


Figure 10.- Variation of motor exit-pressure ratio with Mach number.

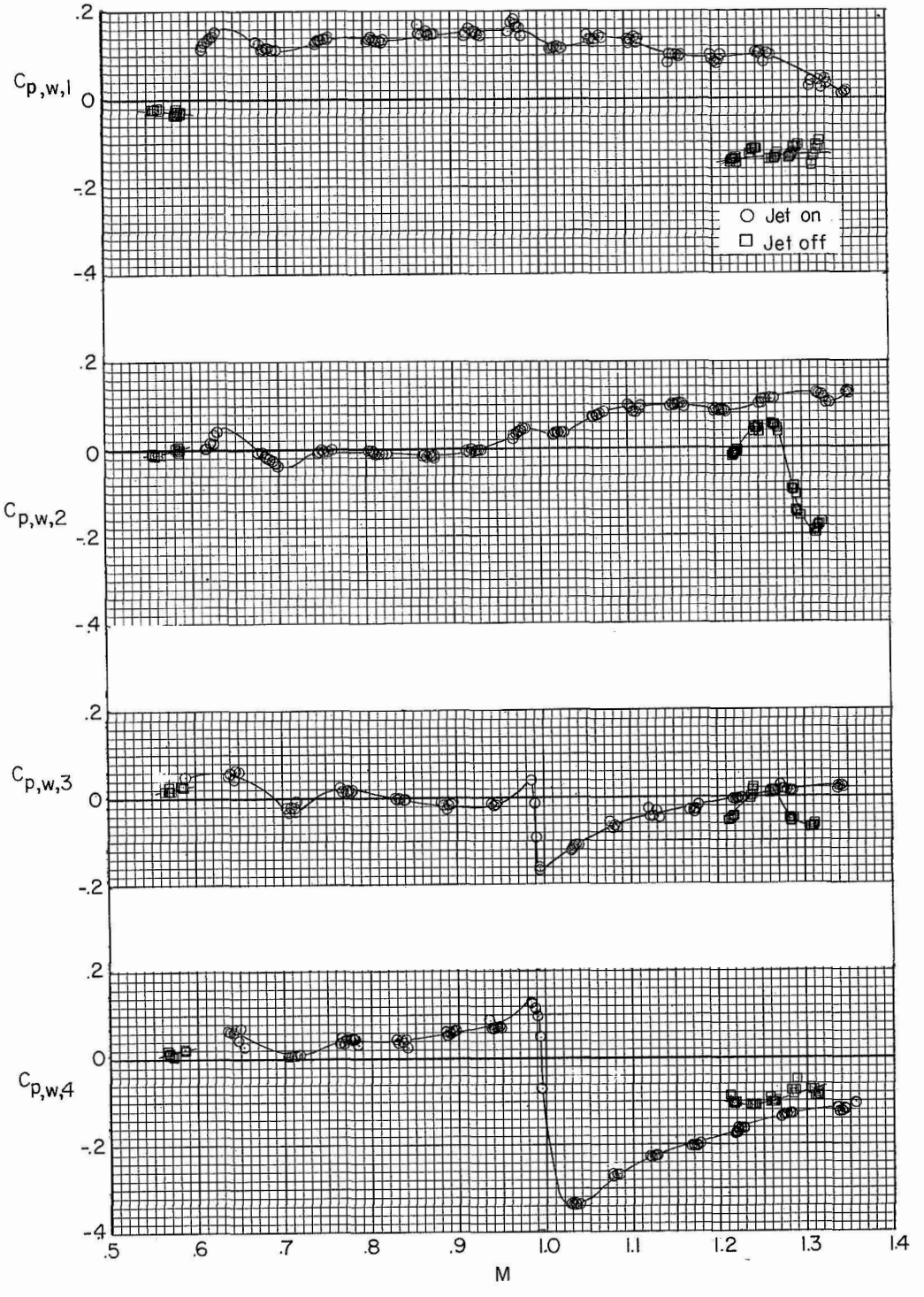


Figure 11.- Variation of wing pressure coefficients with Mach number.

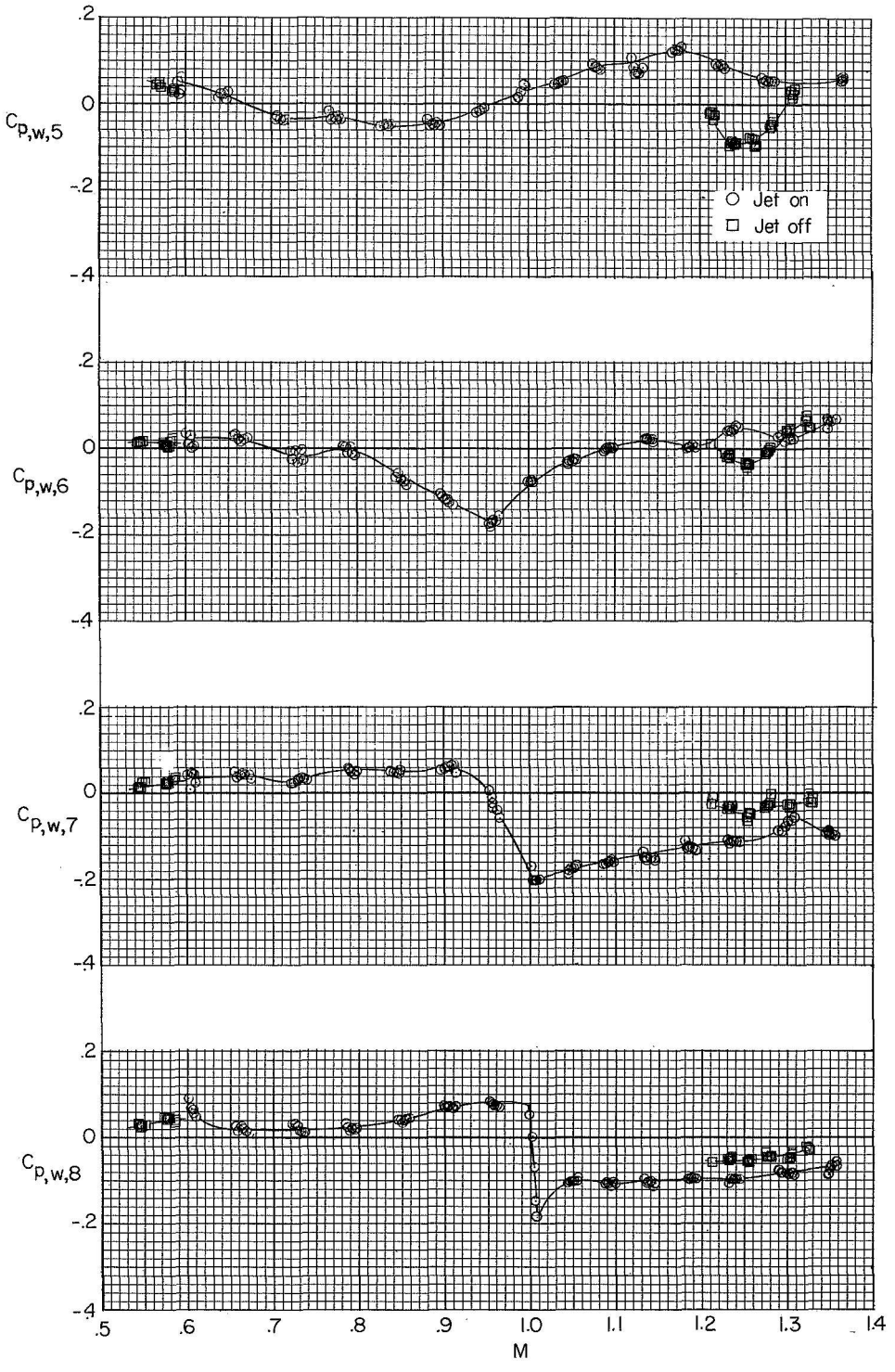
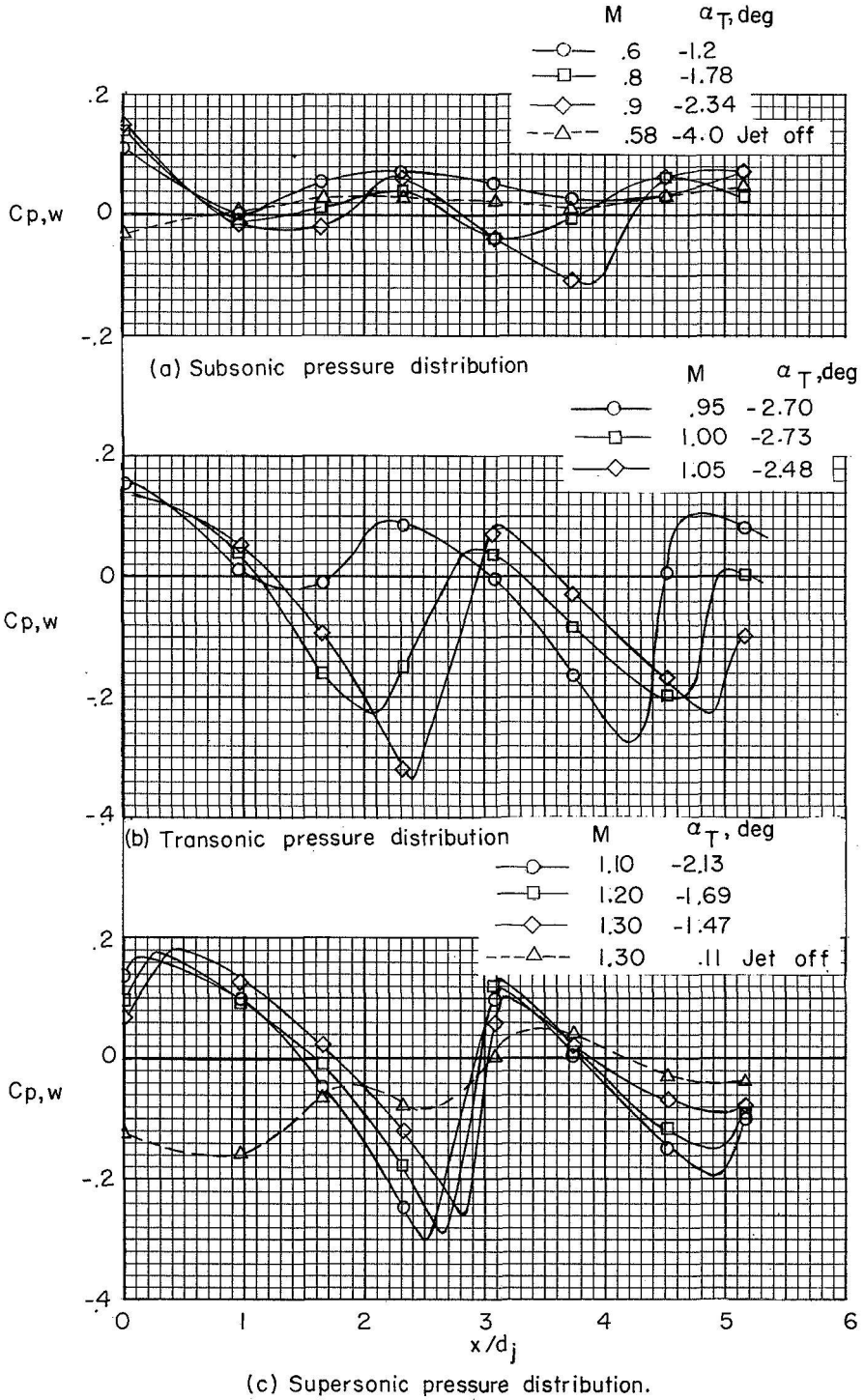


Figure 11.- Concluded.



(c) Supersonic pressure distribution.

Figure 12.- Variation of jet-on and jet-off wing pressure coefficients.

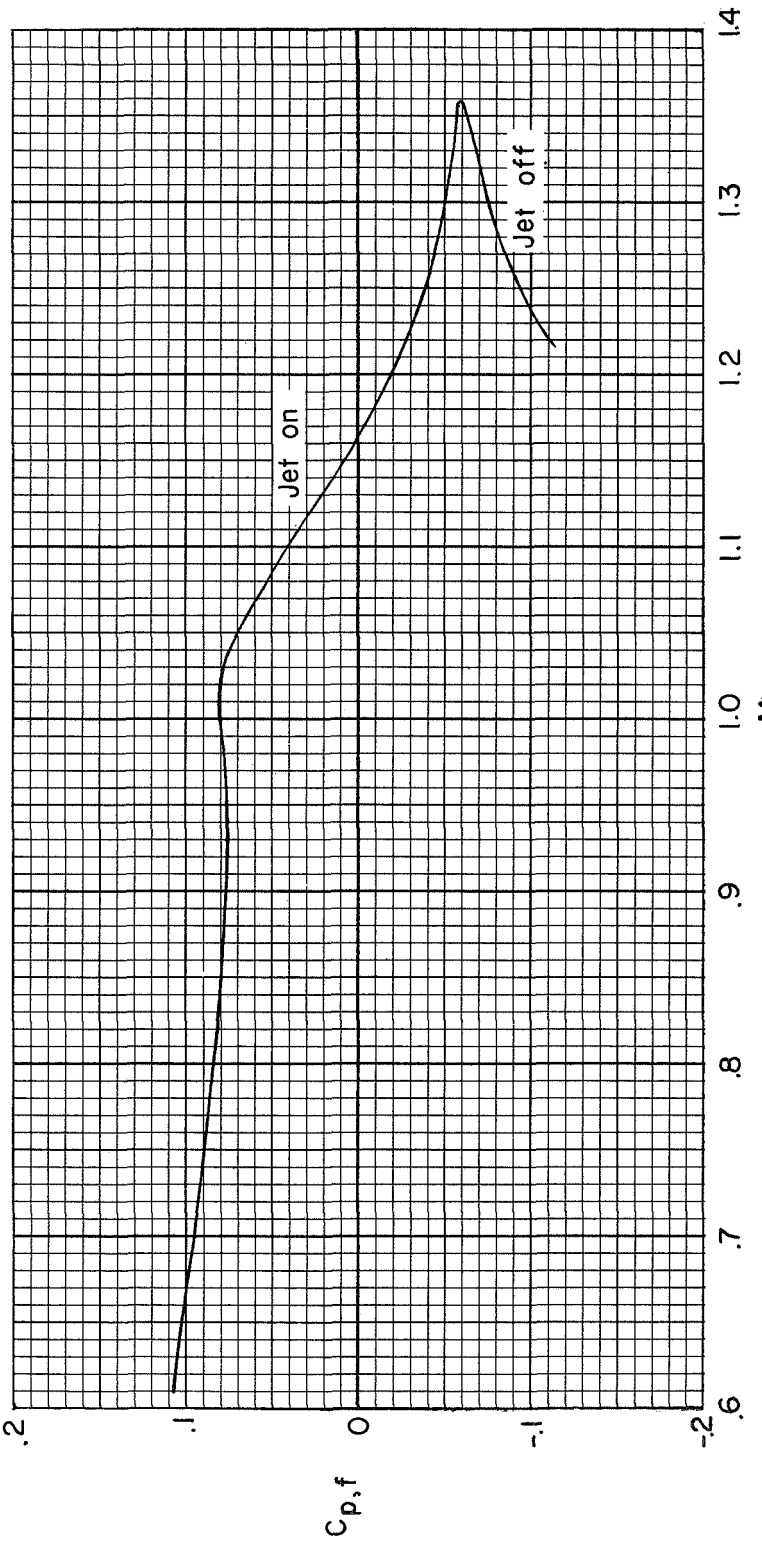
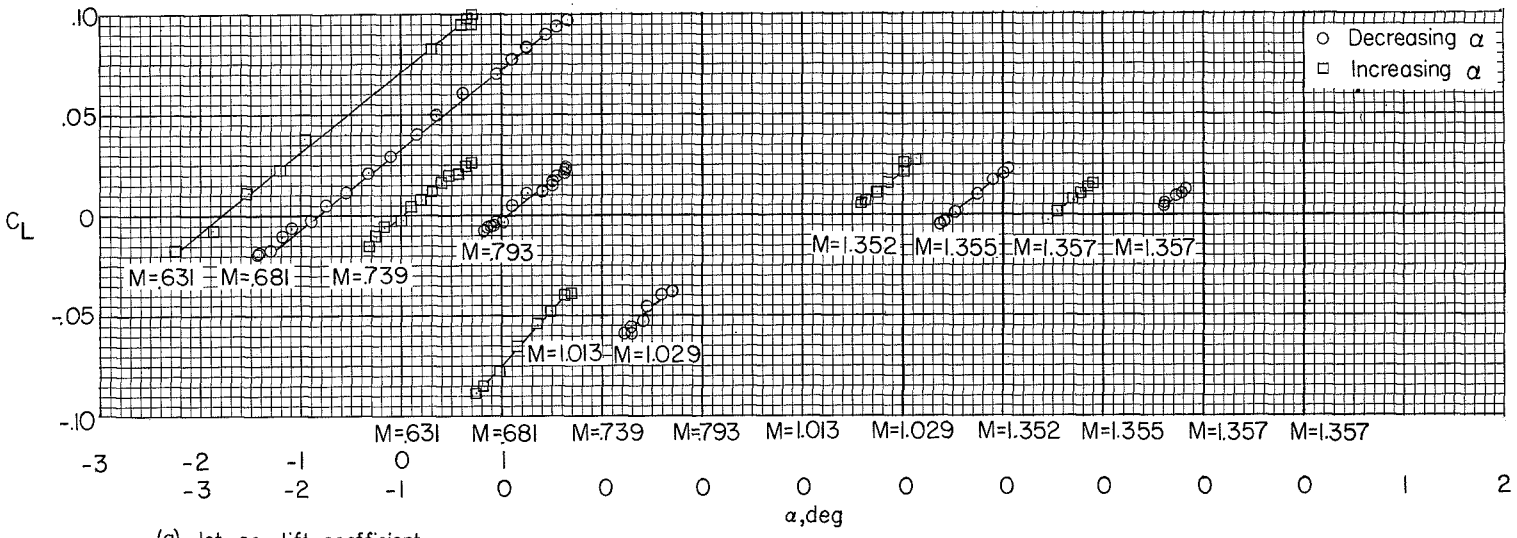
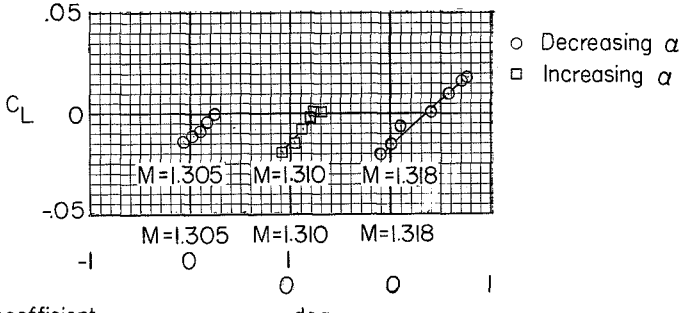


Figure 13.- Variation of fuselage pressure coefficient with Mach number.



(a) Jet on lift coefficient.



(b) Jet off lift coefficient.

Figure 14.- Variation of lift coefficient with angle of attack for jet-on and jet-off flight.

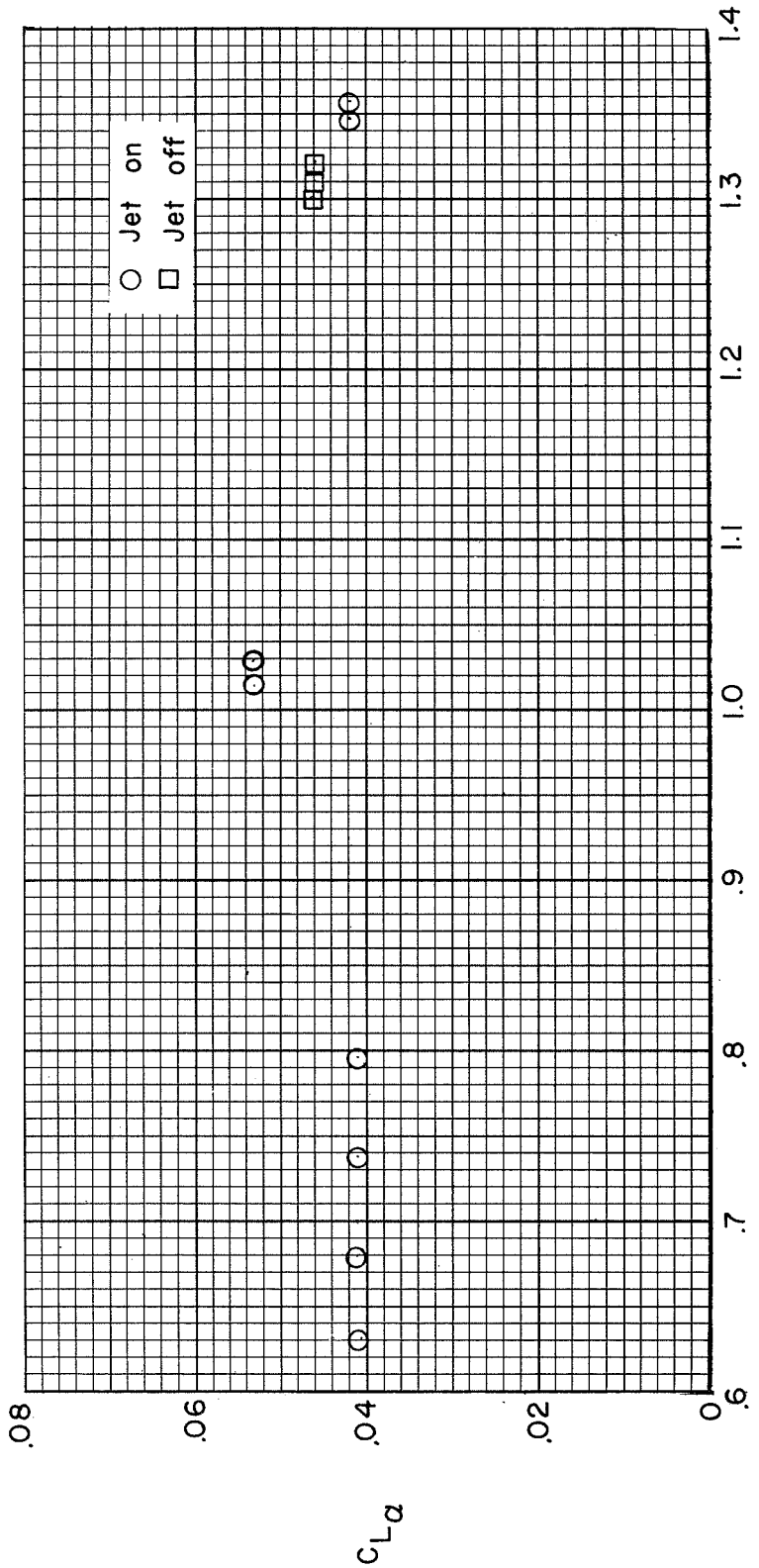


Figure 15.- Variation of lift-curve slope with Mach number.

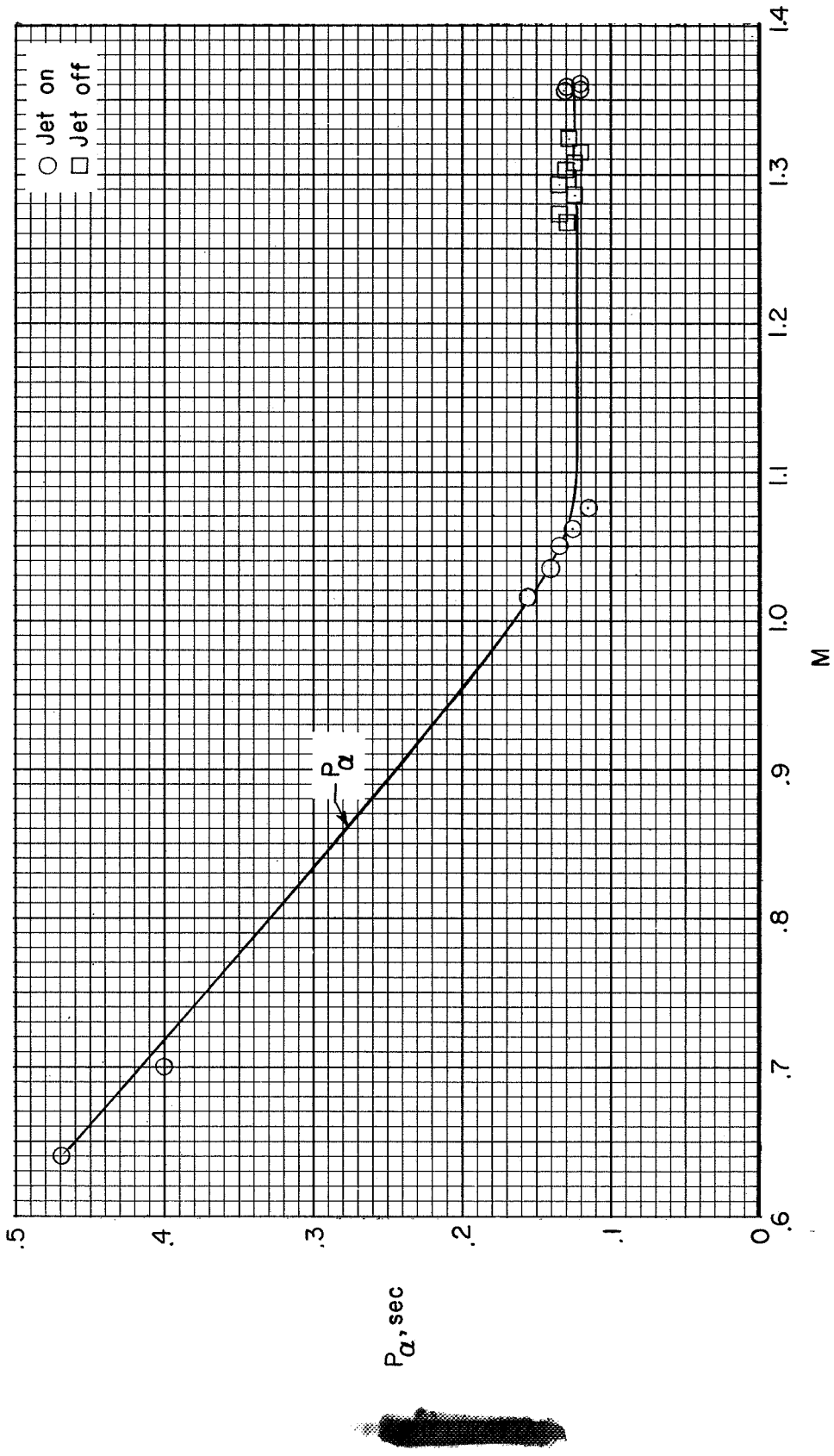


Figure 16.- Variation of pitch period of short-period oscillation with Mach number.

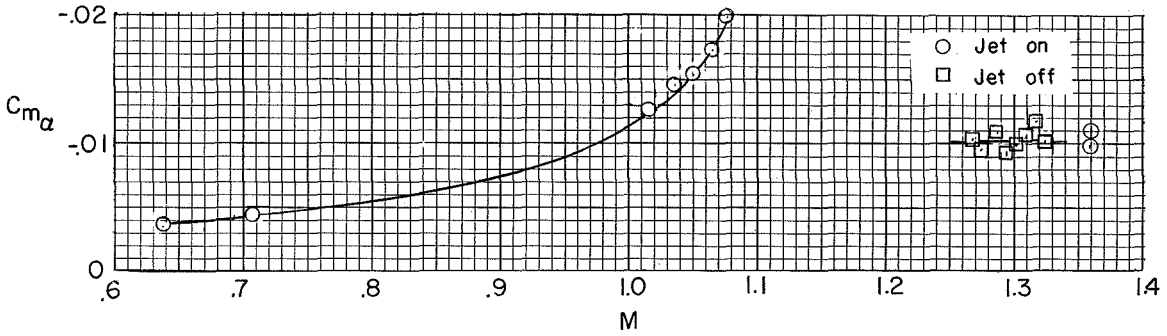


Figure 17.- Variation of pitching-moment-curve slope with Mach number.

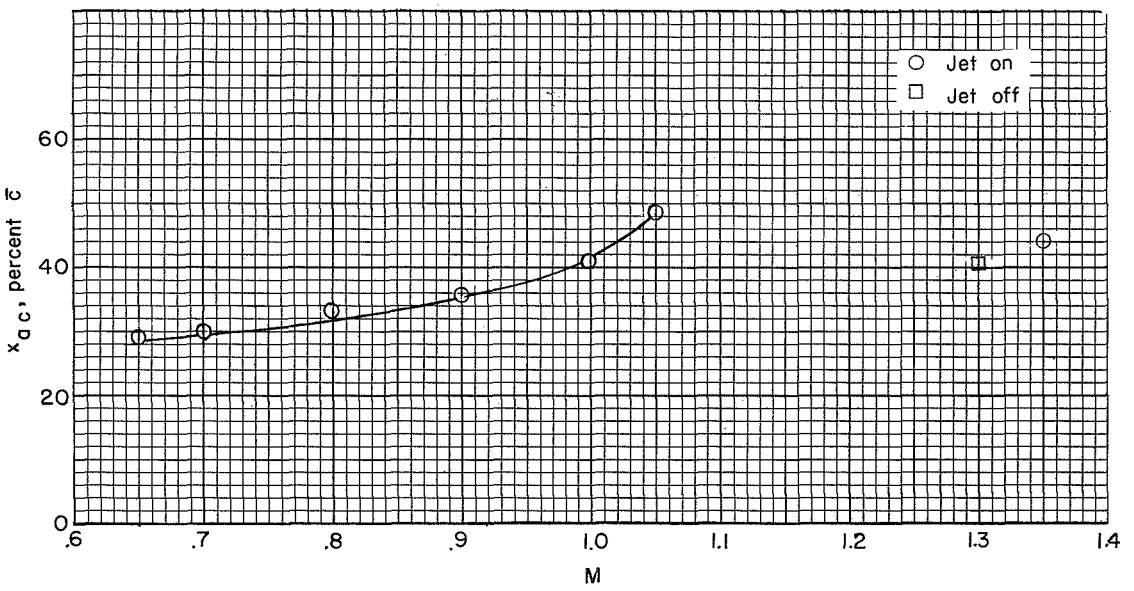


Figure 18.- Variation of aerodynamic center with Mach number.

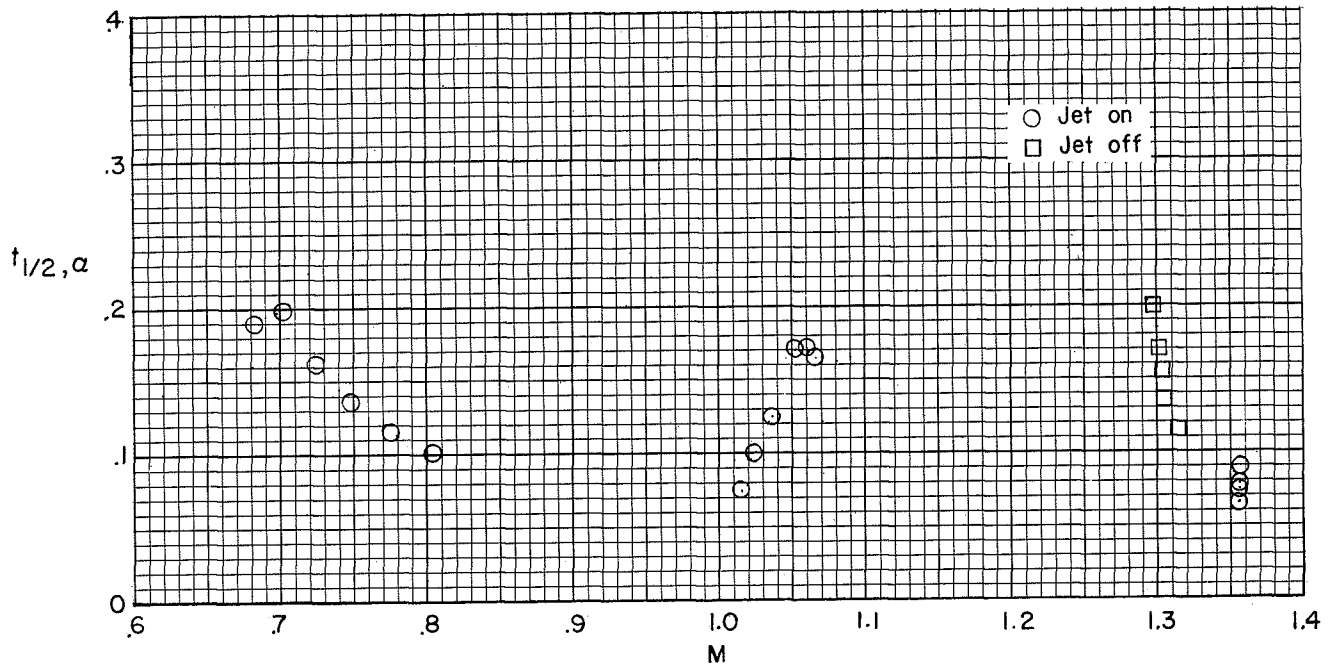


Figure 19.- Variation of time to damp to 1/2 amplitude of the short-period oscillation with Mach number.

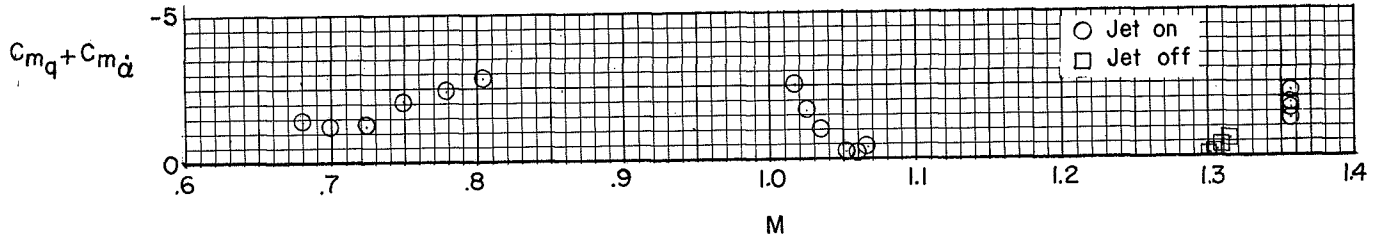


Figure 20.- Variation of damping derivatives in pitch with Mach number.

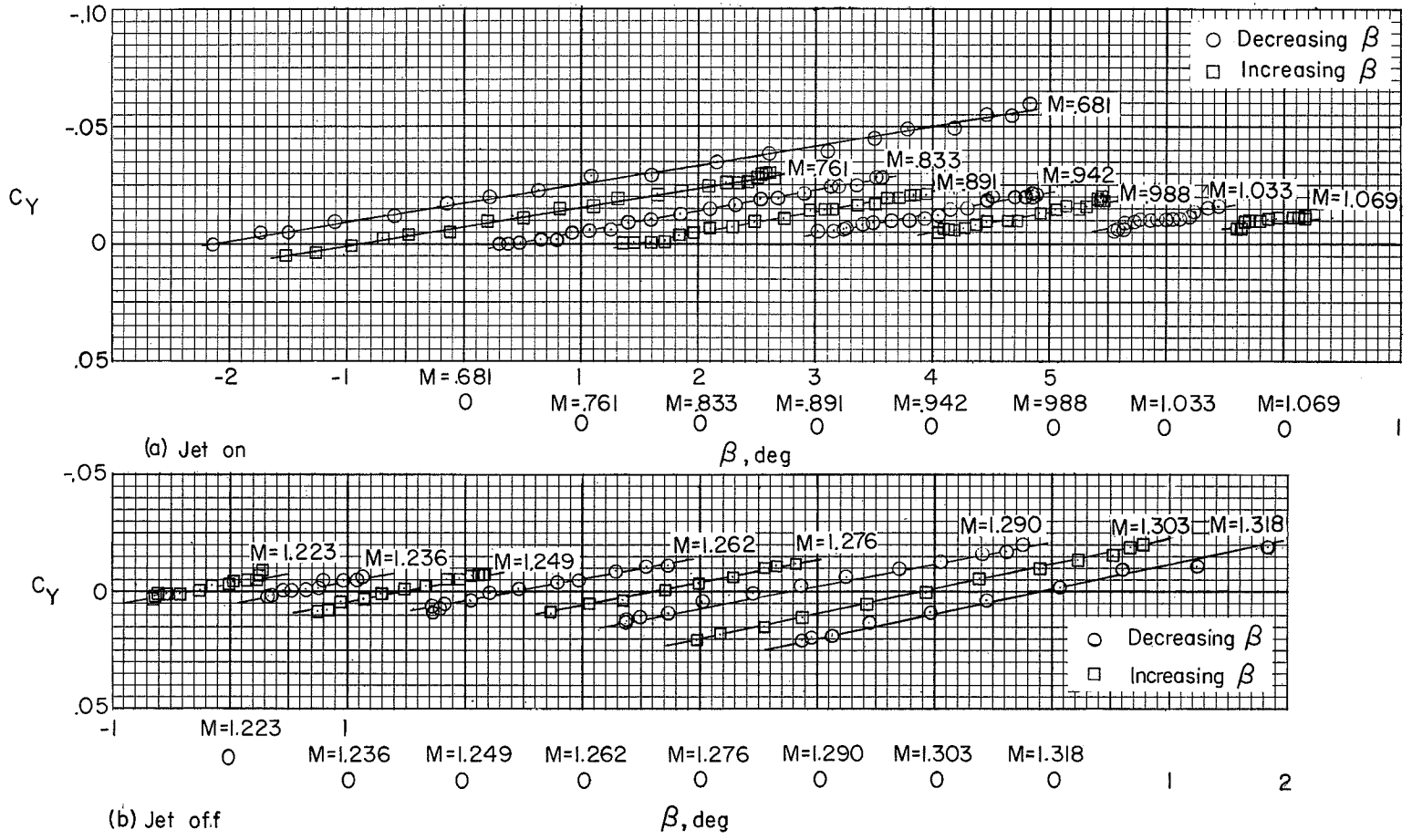


Figure 21.- Variation of lateral force coefficient with angle of yaw for jet-on and jet-off flight.

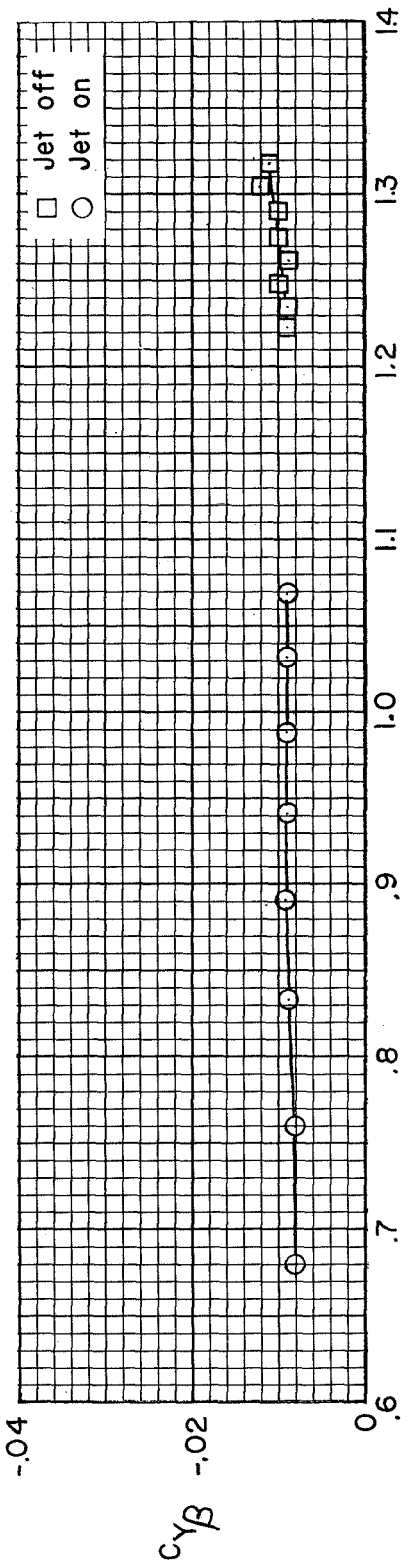


Figure 22.- Variation of lateral-force slope with Mach number.

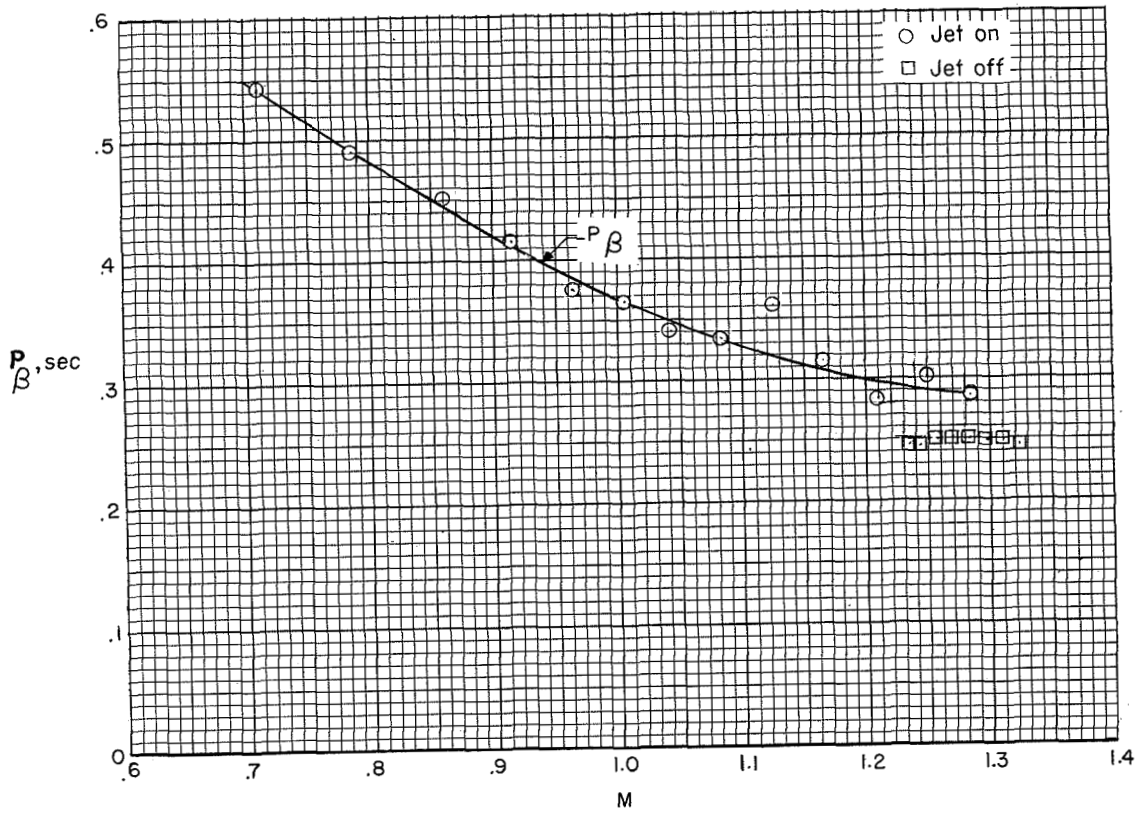


Figure 23.- Variation of yaw period with Mach number.

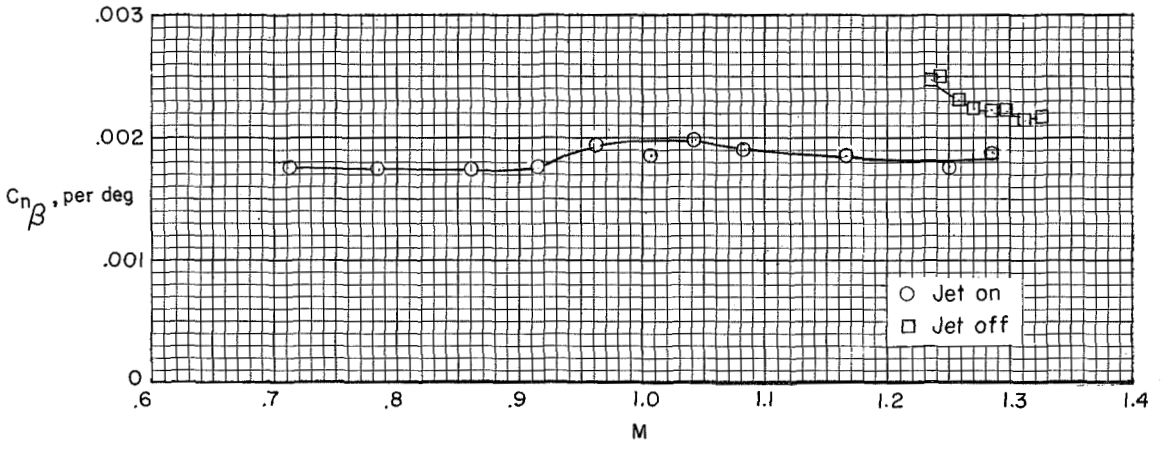


Figure 24.- Variation of directional stability derivative with Mach number.

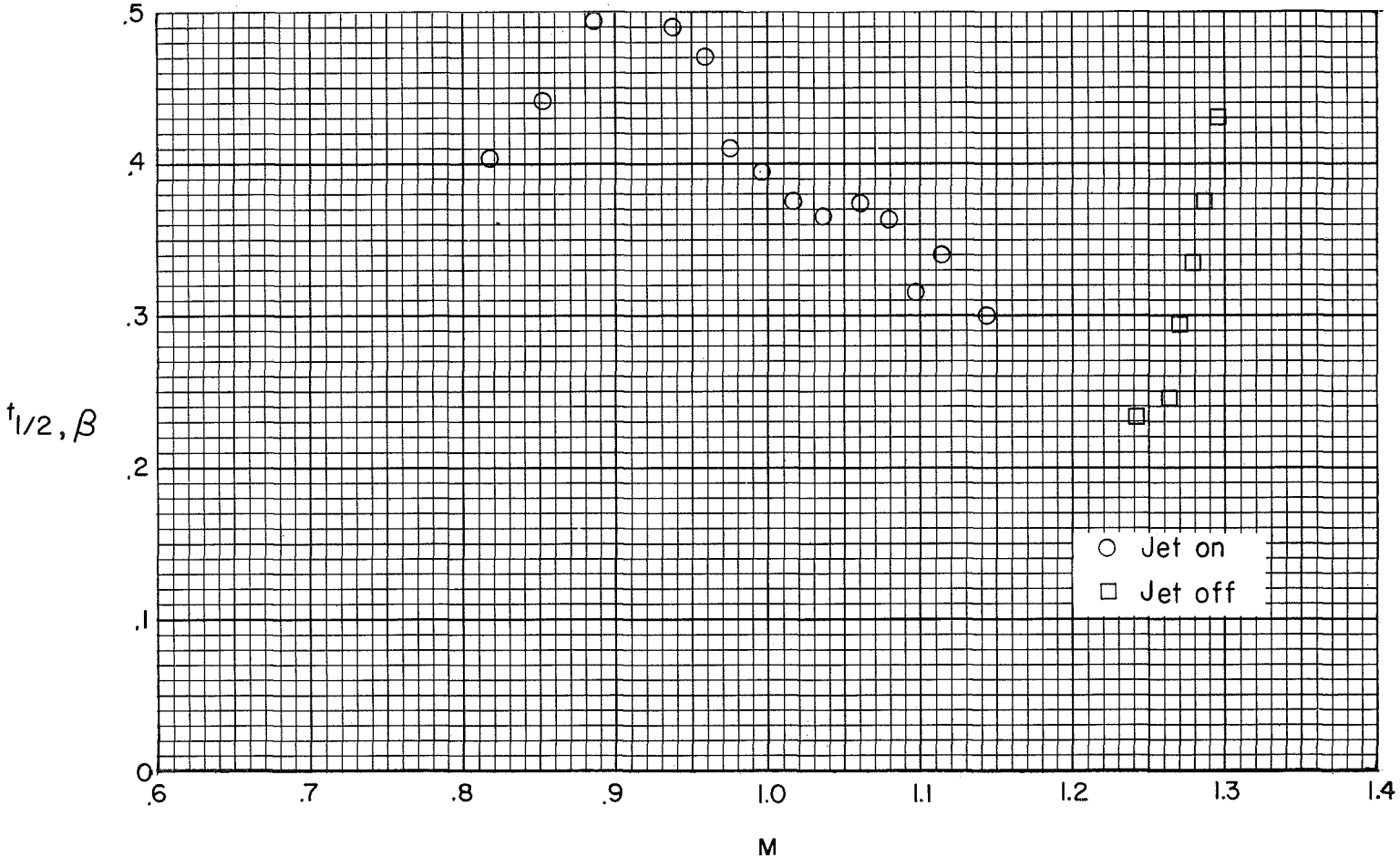
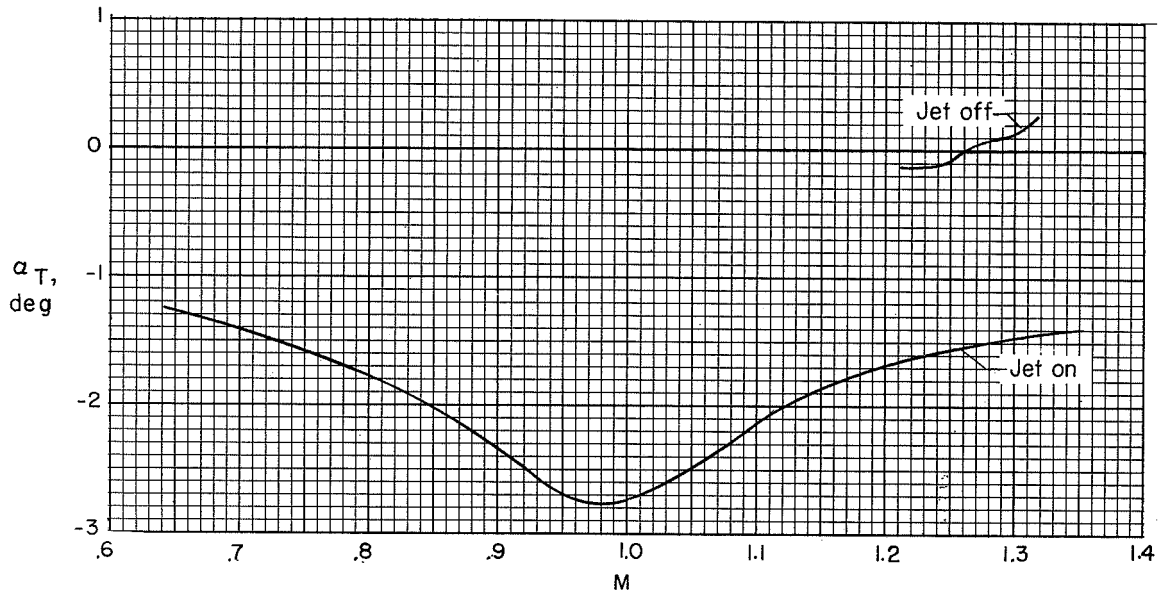
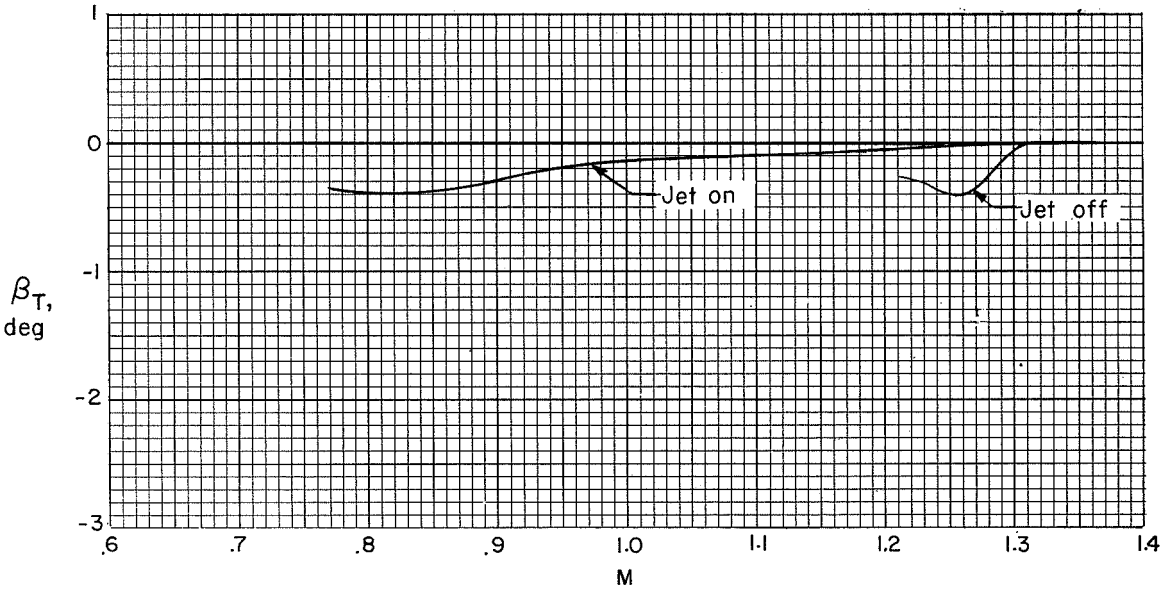


Figure 25.- Variation of time to damp to 1/2 amplitude in yaw with Mach number.

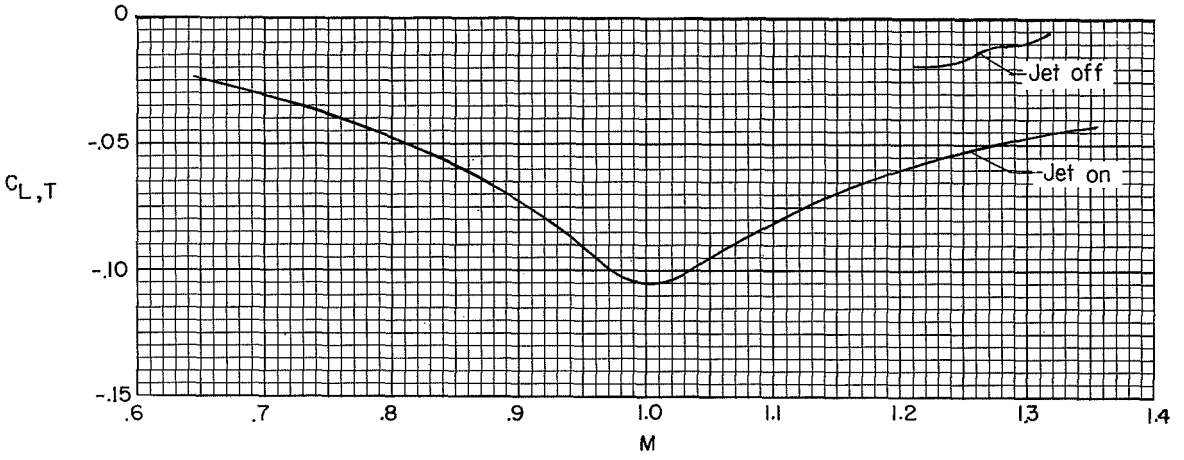


(a) Variation of trim angle of attack with Mach number.

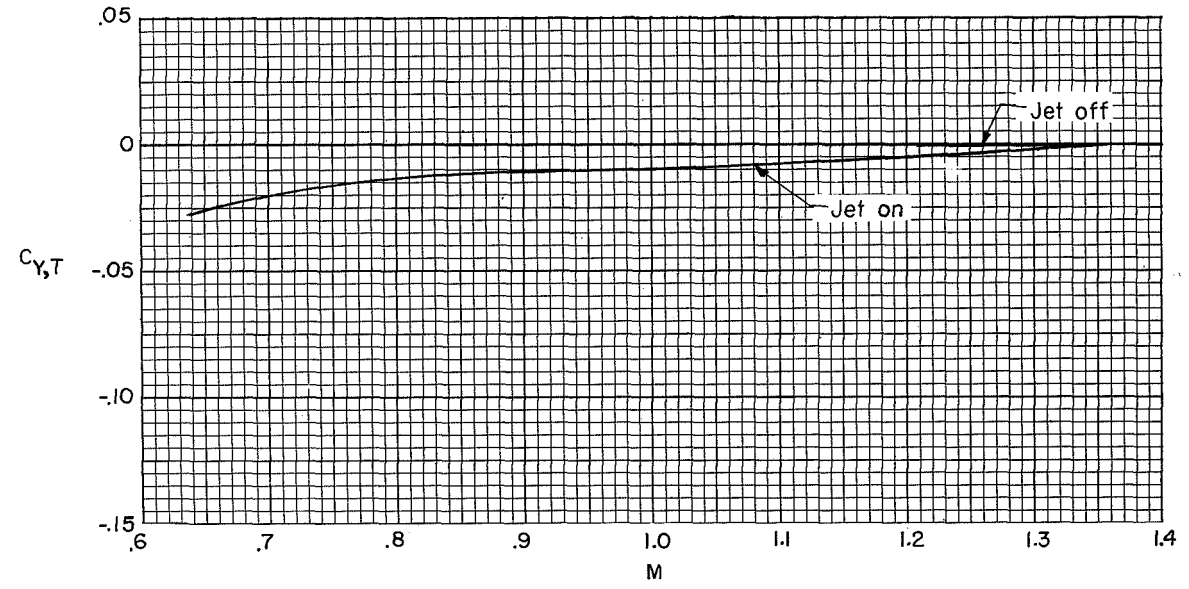


(b) Variation of trim angle of sideslip with Mach number.

Figure 26.- Variation of trim angles with Mach number.



(a) Variation of trim lift coefficient with Mach number.



(b) Variation of trim lateral-force coefficient with Mach number.

Figure 27.- Variation of trim force coefficients with Mach number.